

JGR Atmospheres

RESEARCH ARTICLE

10.1029/2022JD038229

Special Section:

Land-atmosphere coupling: measurement, modelling and analysis

Key Points:

- Our study assesses different biophysical impacts of deforestation on surface temperature in CMIP6 models
- CMIP6 models show wide divergence on the surface temperature changes in the extratropical regions due to non-local atmospheric feedbacks
- Changes in the aerodynamic resistance dominate the surface temperature response to local biophysical effects of deforestation

Supporting Information:

Supporting Information may be found in the online version of this article.

Correspondence to:

W. Hua,
wenjian@nuist.edu.cn





Citation:

Liu, S., Hua, W., Zhou, L., Chen, H., Yu, M., Li, X., & Cui, Y. (2023). Local and non-local biophysical impacts of deforestation on global temperature during boreal summer: CMIP6-lumip multimodel analysis. *Journal of Geophysical Research: Atmospheres*, 128, e2022JD038229. <https://doi.org/10.1029/2022JD038229>

Received 21 NOV 2022

Accepted 26 MAY 2023

Local and Non-Local Biophysical Impacts of Deforestation on Global Temperature During Boreal Summer: CMIP6-LUMIP Multimodel Analysis

Shuyu Liu¹, Wenjian Hua¹ , Liming Zhou² , Haishan Chen¹ , Miao Yu¹ , Xing Li³, and Yazhu Cui¹

¹Key Laboratory of Meteorological Disaster, Ministry of Education (KLME)/Joint International Research Laboratory of Climate and Environment Change (ILCEC)/Collaborative Innovation Center on Forecast and Evaluation of Meteorological Disasters (CIC-FEMD), Nanjing University of Information Science and Technology, Nanjing, China, ²Department of Atmospheric and Environmental Sciences, University at Albany, State University of New York, Albany, NY, USA, ³School of Atmospheric Sciences, Chengdu University of Information Technology, Chengdu, China

Abstract Biophysical effects of forest cover changes are often neglected by climate policies and recent state-of-the-art climate models exhibit wide spreads in simulating the biophysical impacts of deforestation. By using the CMIP6-LUMIP simulations, here we examined the biophysical impacts of deforestation on global temperature and attributed deforestation-induced surface temperature change to different biophysical effects (i.e., radiative forcing, aerodynamic resistance, Bowen ratio and atmospheric feedbacks) at regional scales. Results show that models agree on the sign of temperature responses to different biophysical factors in the tropics, but exhibit wide divergence in the extratropical regions. Among the three local biophysical factors (i.e., radiative forcing, aerodynamic resistance, and Bowen ratio), aerodynamic resistance contributes largely to local surface warming in models. As the local effects rarely affect the areas away from the deforested regions, much of the modeled discrepancies result from non-local atmospheric feedbacks in the middle and high latitudes. Our results suggest that climate responses to deforestation have a large spread in current models and highlight the need to improve our understanding and modeling of non-local effects in the biophysical impacts of deforestation.

Plain Language Summary The Land Use Model Intercomparison Project (LUMIP) multimodel simulations with a common experimental protocol provide a great opportunity to explore the biophysical effects of land use and land cover change and allow a direct comparison of model responses to deforestation. By analyzing the CMIP6-LUMIP multimodel simulations, we show that deforestation causes widespread summer warming in the tropics, but the simulated temperature changes in response to deforestation diverge in the middle and high latitudes. We further attributed deforestation-induced surface temperature change to different biophysical effects (radiative forcing, aerodynamic resistance, Bowen ratio and atmospheric feedbacks). Our results indicate that atmospheric feedbacks play the dominant role in determining the temperature responses, and aerodynamic resistance also matters. The atmospheric feedbacks in the temperate and boreal regions are highly model-dependent. Further efforts to explore the non-local influence of temperate deforestation using state-of-the-art climate models are needed.

1. Introduction

Forests cover almost 42 million km² in the world, occupying over 30% of the Earth's land surface (Bonan, 2008; Luysaert et al., 2014). Since 800 CE, approximately 40% of the land cover (mainly forests) has been modified or converted by human activities into arable land or farmlands for timber, fiber and food (Hurt et al., 2020; Pongratz et al., 2008). As one of the main drivers of land cover change (Khanna et al., 2017; Tölle et al., 2017; Werth & Avissar, 2002), deforestation (e.g., resulting from the expansion of agriculture and logging) has strong implications for the hydrological cycle, energy budget and terrestrial carbon stocks (Lawrence & Vandecar, 2015; Runyan et al., 2012; Spracklen et al., 2018; Yuan et al., 2021). A comprehensive understanding of the impacts of deforestation on the climate system is therefore of significant environmental importance and is crucial for future land management policy (Pongratz et al., 2021).

Forests influence climate through biophysical and biogeochemical processes (Bathiany et al., 2010; Bonan, 2016; Claussen et al., 2001; Ge et al., 2019; Pongratz et al., 2010). In terms of biophysical mechanisms, deforestation causes changes in a range of surface properties (e.g., albedo, aerodynamic roughness, leaf area index, and water availability), and subsequently modifies the energy and water fluxes across the land-atmosphere interface (Foley et al., 2005; Mahmood et al., 2014; Perugini et al., 2017; Pielke et al., 2011). In general, deforestation increases albedo, resulting in less solar radiation absorbed by the surface (Hua & Chen, 2013) and suppresses evapotranspiration because forests have larger leaf areas and root depths than other vegetation types (Betts et al., 2007; Breil et al., 2021). Deforestation also decreases aerodynamic roughness and consequently changes turbulent fluxes (e.g., sensible and latent heat fluxes) (Burakowski et al., 2018; Chen et al., 2020; Zhao & Jackson, 2014; Zhou et al., 2007). The biogeochemical effects are primarily linked to changes in the carbon cycle (Liu et al., 2013, 2015; Van Marle et al., 2016) and deforestation may increase the emissions of CO₂ into the atmosphere (Houghton & Hackler, 2003; Hua et al., 2015; Van der Werf et al., 2009), and accelerate global warming (Di Vittorio et al., 2018). Thus, afforestation (e.g., carbon capture and storage) could help mitigate climate change (Griscom et al., 2017; Jackson et al., 2008). However, gains from carbon sinks may be offset by the biophysical effects (Alkama & Cescatti, 2016; Betts, 2000; Huang et al., 2020; Lee et al., 2011; Li, de Noblet-Ducoudré et al., 2016; Rotenberg & Yakir, 2010).

Previous observational studies have suggested that the net biophysical impacts of deforestation on global temperature depends on the competing effects of albedo, evapotranspiration (ET) and roughness length (Duveiller et al., 2018; Li et al., 2015). This is used to explain why the temperature response is reversed from the tropical to temperate and boreal forests (Li, Zhao, et al., 2016; Zhang et al., 2014). However, observationally based methods (i.e., space-for-time approach), which compare neighboring land units with contrasting land cover types (e.g., forests vs. open lands) to extract local impacts of deforestation by assuming similar atmospheric conditions, ignore possible non-local atmospheric feedbacks or heterogeneous land-atmosphere interactions over different land covers (Chen & Dirmeyer, 2020; Hirsch et al., 2014). Likely, the non-local biophysical effects driven by regional to large scale atmospheric thermodynamic and dynamic processes are probably not captured by observational methods (Winckler, Lejeune, et al., 2019). Many studies have used climate models to detect the impacts of deforestation (Bala et al., 2007; Davin & De Noblet-Ducoudré, 2010; Devaraju et al., 2018; Lejeune et al., 2018). Results from the CMIP5 (Coupled Model Intercomparison Project Phase 5, Kumar et al., 2013; Lejeune et al., 2017), LUCID (Land-Use and Climate, IDentification of robust impacts, Pitman et al., 2009; de Noblet-Ducoudré et al., 2012), and LUCAS (Land Use and Climate Across Scales; Davin et al., 2020) multimodel experiments documented a large spread in climate responses to deforestation.

Recently, the Land Use Model Intercomparison Project (LUMIP, Lawrence et al., 2016) multimodel simulations, which were part of the Coupled Model Intercomparison Project Phase 6 (CMIP6, Eyring et al., 2016), were conducted to understand the impacts of land use and land cover change (LULCC) on climate (Boysen et al., 2020; Luo et al., 2022). Boysen et al. (2020) first utilized the CMIP6-LUMIP multimodel simulations to examine the biophysical effect of large scale deforestation and found that the impacts of deforestation vary in sign (i.e., a switch of sign from tropical warming to extratropical cooling located around 22.6°N). Furthermore, not only the radiative and non-radiative effects associated with albedo, roughness length and ET efficiency play an important role in determining the local biophysical impacts of deforestation (e.g., Lee et al., 2011; Li et al., 2015), but the non-local atmospheric feedbacks are also important (Boisier et al., 2012; Chen & Dirmeyer, 2020; Devaraju et al., 2018). Deforestation could indirectly trigger non-local biophysical impacts, through advection of heat and moisture and via changes in atmospheric circulation (e.g., Bala et al., 2007; Devaraju et al., 2015; Portmann et al., 2022). Thus, the relative contributions of different local versus non-local biophysical effects (e.g., Winckler, Lejeune, et al., 2019) may alter the sign and magnitude of temperature responses geographically (Boisier et al., 2012; Devaraju et al., 2018) and differ across the state-of-the-art climate models participating in CMIP6 (Boysen et al., 2020).

In this study, we used a revised intrinsic biophysical mechanism (IBPM) approach to separate the biophysical effects of deforestation into different components (e.g., radiative forcing, aerodynamic resistance, Bowen ratio and atmospheric feedbacks) (Chen & Dirmeyer, 2016; Liao et al., 2018). This IBPM approach has commonly used to examine the individual biophysical impacts of deforestation in observational (in situ and remote sensing) data, offline land surface model simulations and CMIP5 models. Here we used this decomposition method to comprehensively examine the biophysical impacts of deforestation on global temperature through analyses of CMIP6-LUMIP multimodel simulations. As ET-induced warming (cooling) due to deforestation (afforestation

Table 1
LUMIP Experimental Design and Description (Lawrence et al., 2016)

Experiment ID	Experiment description	Years
Deforest-globe	Idealized global deforestation experiment, with a period of 50 years as the idealized deforestation scenario and the last 30 years as a constant state	≥80
piControl	All external forcings (including CO ₂ concentration and land use and land management) maintained at the 1850 years	≥500

and vegetation greening) is most prominent in summer (Li et al., 2015; Lian et al., 2022) and land surface models have difficulties in realistically simulating snow-albedo feedback over forested surfaces (Lorantý et al., 2014; Thackeray et al., 2019; Zhou et al., 2003), we focused on the boreal summer season of June–July–August (JJA). First, we examine the temperature changes and surface energy fluxes at global and regional scales. Second, we quantify the relative contributions of different biophysical effects on surface temperature in response to deforestation using the energy balance decomposition method. Third, we investigate the inter-model variations of deforestation-driven changes and reveal the possible biophysical effects for the inter-model spread. Section 2 describes the model simulations from the CMIP6-LUMIP and methods. The results are presented in Section 3, followed by discussions in Section 4. Section 5 concludes with a brief summary of the findings.

2. Data and Methods

2.1. CMIP6-LUMIP Experiments

We analyzed the model simulations from the CMIP6-LUMIP. LUMIP was designed to address scientific questions related to land-use, including the impacts of LULCC on climate and biogeochemical cycling and influence of various aspects of land management on surface fluxes of energy, water and carbon, and interactions and feedbacks between climate change and land use change. LUMIP includes a two-phase, tiered design framework (Lawrence et al., 2016). We used the phase one experiment with an idealized deforestation scenario (i.e., deforest-globe). The deforest-globe simulation is branched from the pre-industrial control (piControl, with all forcing kept at the 1,850 level) simulation and runs for at least 80 years. In the deforest-globe, 20 million km² of forest area is converted to natural grassland with a linear rate of decline of 400,000 km² over a period of 50 years, followed by 30 years of constant forest cover. In this simulation, all external forcings except the forest cover changes are the same as in piControl (Table 1). A detailed description of the LUMIP experiments is given by Lawrence et al. (2016).

In order to reduce the influence of internal climate variability or model “noise,” we used three CMIP6 models, with the number of realizations greater than or equal to three (Table S1 in Supporting Information S1). These models are CESM2 (Danabasoglu et al., 2020), IPSL-CM6A-LR (Boucher et al., 2020) and MPI-ESM1-2-LR (Mauritsen et al., 2019). Both CESM2 and IPSL-CM6A-LR have three members and run for 80 years, while MPI-ESM1-2-LR has seven members and runs for 150 years. Figure 1 shows the total fractional changes in forest cover in the deforest-globe simulations for the three models. We used the differences in the forest fraction between the final year and the first time step to represent the deforestation pattern. Since deforestation only occurs in the top 30% of land grid cells with the highest fractional forest cover in the model simulations (Lawrence et al., 2016), the significant forest reductions are found in South America, Central Africa, Eurasia and North America (Figures 1a–1c). Note that the deforest-globe simulations are initialized from their pre-industrial control runs and the initial fraction of forest cover in each model is slightly different. Thus, the deforestation patterns exhibit small differences (Figures 1a–1c).

2.2. Methods

As the ground biomass or the carbons from the forested soil due to idealized deforestation are not considered in the models, deforestation only influences global climate through biophysical processes. To investigate the biophysical effects of deforestation, we used the piControl simulations to serve as a reference. The biophysical deforestation effects were then computed as the differences between the deforest-globe and piControl simulations. To assess the statistical significance of the difference between these two simulations, a modified two-sided Student's *t* test was applied in this study (Zwiers & Von Storch, 1995). In the deforest-globe, the first 50 years

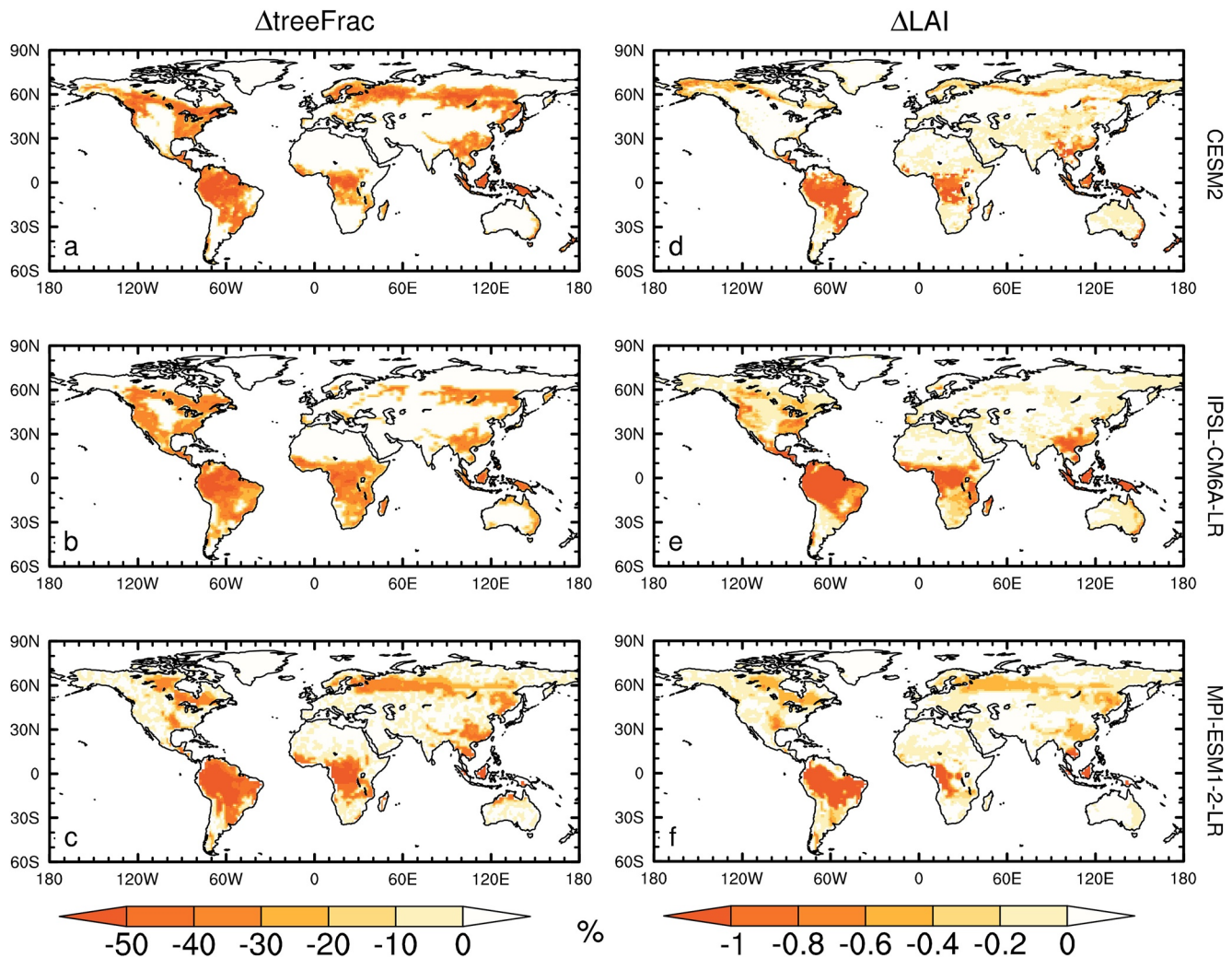


Figure 1. (a)–(c) Fractional changes (%) in forest cover and (d)–(f) differences in LAI ($\text{m}^2 \text{m}^{-2}$) in the deforest-globe simulations for (a), (d) CESM2, (b), (e) IPSL-CM6A-LR and (c), (f) MPI-ESM1-2-LR models. We used the difference between the final year and the first time step in the deforest-globe simulations to represent the forest cover and LAI changes.

are considered as biophysical spin-up and the last 30 years (for all the three models) are used for analysis. We analyzed the ensemble mean of these three model simulations and focused on the summer season (i.e., JJA). All the model data sets were regrided onto a common $1^\circ \times 1^\circ$ grid using bilinear spatial interpolation, in order to facilitate inter-model comparisons. To examine the regionally aggregated responses to deforestation, four densely forested regions are selected, including South America (30°S – 12°N , 40 – 82°W), Central Africa (17°S – 11°N , 8° – 35°E), Eurasia (55 – 70°N , 35 – 95°E), and North America (45 – 60°N , 50 – 135°W).

To understand the biophysical impacts of deforestation on surface temperature, we introduced a decomposition method derived from the intrinsic biophysical mechanism (IBPM, Chen & Dirmeyer, 2016; Lee et al., 2011; Liao et al., 2018; Li et al., 2022). In this way, we can disentangle relative contributions of different biophysical impacts of deforestation (e.g., radiative forcing, aerodynamic resistance, Bowen ratio and atmospheric feedbacks) on surface temperature. According to the surface energy budget equation, the net surface radiation (R_n , W m^{-2}) can be decomposed into the following form:

$$R_n = S + \epsilon LW_{\text{down}} - \epsilon \sigma T_s^4 = H + LE + G, \quad (1)$$

where S is net surface shortwave radiation (W m^{-2}), LW_{down} is incoming longwave radiation (W m^{-2}), ϵ is surface emissivity, σ is the Stefan-Boltzmann constant (approximately equal to $5.671 \times 10^{-8} \text{ W m}^{-2} \text{ K}^{-4}$), T_s is surface

temperature (K), H is sensible heat flux (W m^{-2}), LE is latent heat flux (W m^{-2}), and G is ground heat flux (W m^{-2}). The sensible and latent heat fluxes are defined as:

$$H = \rho C_p \frac{T_s - T_a}{\gamma_a}, \quad (2)$$

$$LE = \frac{H}{\beta}, \quad (3)$$

where ρ is air density (kg m^{-3}), C_p is specific heat content ($\text{J kg}^{-1} \text{K}^{-1}$), T_a is air temperature at 2-m reference height (K), γ_a is aerodynamic resistance (s m^{-1}), and β is Bowen ratio.

Linearizing the surface outgoing longwave radiation in Equation 1 using a Taylor series expansion with T_a :

$$T_s^4 = T_a^4 + 4T_a^3(T_s - T_a), \quad (4)$$

Using Equations 2–4, T_s can be given as:

$$T_s = \frac{\lambda_0}{1+f} (R_n^* - G) + T_a, \quad (5)$$

where $\lambda_0 = \frac{1}{4\sigma T_a^3}$, $f = \frac{\rho C_p}{4\sigma T_a^3 \gamma_a} \left(1 + \frac{1}{\beta}\right)$, λ_0 represents the temperature sensitivity and f is the energy redistribution factor. R_n^* is apparent net radiation ($R_n^* \approx R_n$; W m^{-2}).

As the IBPM approach assumes the same atmospheric background for contrasting land cover types (e.g., comparing neighboring open lands with contrasting forests to extract impacts of deforestation), changes in T_a and G are neglected. Surface temperature change ΔT_s (e.g., changes induced by deforestation) can be given by the first derivative of Equation 5:

$$\Delta T_s \approx \frac{\lambda_0}{1+f} \Delta S + \frac{\lambda_0}{(1+f)^2} R_n \Delta f, \quad (6)$$

where ΔS is the change of net surface shortwave radiation, and Δf is the change in the energy redistribution factor due to changes in aerodynamic resistance (Δf_1), and Bowen ratio (Δf_2):

$$\Delta f_1 = -\frac{\rho C_p}{4\sigma T_a^3} \left(1 + \frac{1}{\beta}\right) \frac{\Delta \gamma_a}{\gamma_a^2}, \quad (7)$$

$$\Delta f_2 = -\frac{\rho C_p}{4\sigma T_a^3 \gamma_a} \frac{\Delta \beta}{\beta^2}, \quad (8)$$

Note that the IBPM approach (Lee et al., 2011) does not consider the non-local atmospheric feedbacks from LULCC (Chen & Dirmeyer, 2020; Hirsch et al., 2014). The changes in the atmospheric background state and G cannot be ignored for large scale deforestation. Therefore, Equation 6 is revised as follows (Chen & Dirmeyer, 2016; Liao et al., 2018):

$$\Delta T_s \approx \frac{\lambda_0}{1+f} (\Delta R_n - \Delta G) + \frac{-\lambda_0}{(1+f)^2} (R_n - G) \Delta f_1 + \frac{-\lambda_0}{(1+f)^2} (R_n - G) \Delta f_2 + \Delta T_a + \epsilon 1, \quad (9)$$

where ΔT_a is the change in air temperature. In Equation 9, the right-hand side of the equation represents the contributions of radiative forcing, aerodynamic resistance, Bowen ratio, atmospheric feedbacks and residual components to T_s changes, respectively. The first three terms (i.e., radiative forcing, aerodynamic resistance, and Bowen ratio) represent the local biophysical effects, which are related to the changes in physical properties of the land surface and surface energy balance (Pongratz et al., 2021). In the real atmosphere, the actual temperature depends not only on the radiative forcing, but also on energy redistribution through convection, evaporation, and turbulence in the atmospheric boundary layer (ABL). Thus, Bowen ratio has been used to reflect the relative magnitudes of sensible and latent heat fluxes as well as the land surface thermal-hydrologic properties. The fourth term (i.e., atmospheric feedbacks) generally represents the biophysical effects due to the changes in heat and moisture advection and atmospheric circulation (Chen & Dirmeyer, 2020; Winckler et al., 2017). The last

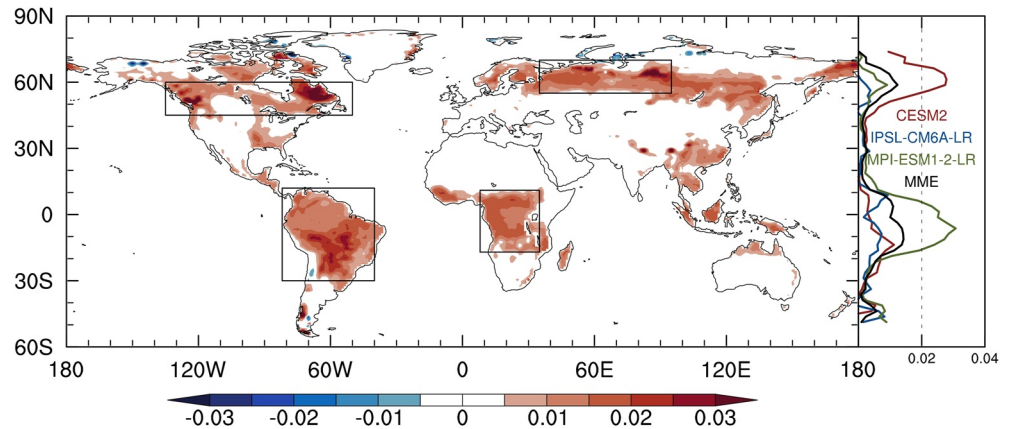


Figure 2. Spatial pattern of JJA surface albedo from the multi-model ensemble mean (MME) of deforest-globe simulations relative to piControl simulations. Also shown are the zonal-averaged changes in surface albedo due to deforestation in the three model simulations. The black line (right panel) represents the MME of these three model results. The outlined boxes (i.e., Central Africa, South America, North America, and Eurasia), which show greatest albedo changes in deforested regions, are analyzed further below.

term ε_1 denotes the errors from missing components (e.g., changes in T_s due to other factors and higher-order interactions ignored here).

This decomposition method implicitly assumes that these biophysical factors are independent of each other, although the non-linear effects (e.g., interactions among these terms) cannot be fully captured in the linearization processes. For example, an increase in Bowen ratio (or aerodynamic resistance) increases T_s . T_a represents the interactions of the air at 2-m height with the boundary layer, the surface, and the free atmosphere. Its changes may influence the atmospheric circulation or the distribution of cloud and precipitation locally and remotely (e.g., vegetation feedback; Wang et al., 2011; Yu et al., 2016), which in turn affects surface temperature via radiative and non-radiative processes.

3. Results

3.1. Impacts on Summer Temperatures

Changes in land cover types can affect surface biophysical properties, such as leaf area index (LAI), surface albedo and canopy roughness (Bonan, 2008). We first examined the changes in LAI in the idealized global deforestation experiments (Figures 1d–1f). LAI is a key variable describing plant canopy structure and is used as a measure of forest growth globally (Forzieri et al., 2017; Zeng et al., 2017). In the deforest-globe, LAI is expected to decrease in tropical and temperate regions when forests are replaced by grasslands. LAI decline is more significant in the tropics where the initial LAI is higher than other areas and the main cover type is broadleaf forest. Furthermore, LAI also decreases in north borders of temperate regions, in particular in CESM2 and MPI-ESM1-2-LR (Figures 1d–1f).

Figure 2 shows the spatial pattern of surface albedo changes due to deforestation. In general, surface albedo is higher when replacing forests by grasses. This could lead to a cooling effect through the reduction in solar radiation absorbed by the surface associated with increased surface albedo. The albedo increases are more remarkable in South America, Central Africa, and the mid-latitudes of Eurasia and North America (Figure 2). In terms of zonally average variations, the changes in surface albedo are consistent among these models, with remarkable increases in tropical and boreal regions. However, there exist some differences in the magnitude of albedo change among the models, with the most significant increases in the tropics in MPI-ESM1-2-LR, but the greatest changes in the mid to high northern latitudes in CESM2.

Note that the replacement of trees by natural grasslands leads to an increase in surface albedo and a decrease in vegetation transpiration and roughness length. These changes contribute to increases in outgoing shortwave radiation (radiative processes) and decreases in turbulent fluxes (non-radiative processes), both of which have a strong latitudinal and seasonal dependence (Alkama & Cescatti, 2016; Lee et al., 2011; Li et al., 2015). The net effect of

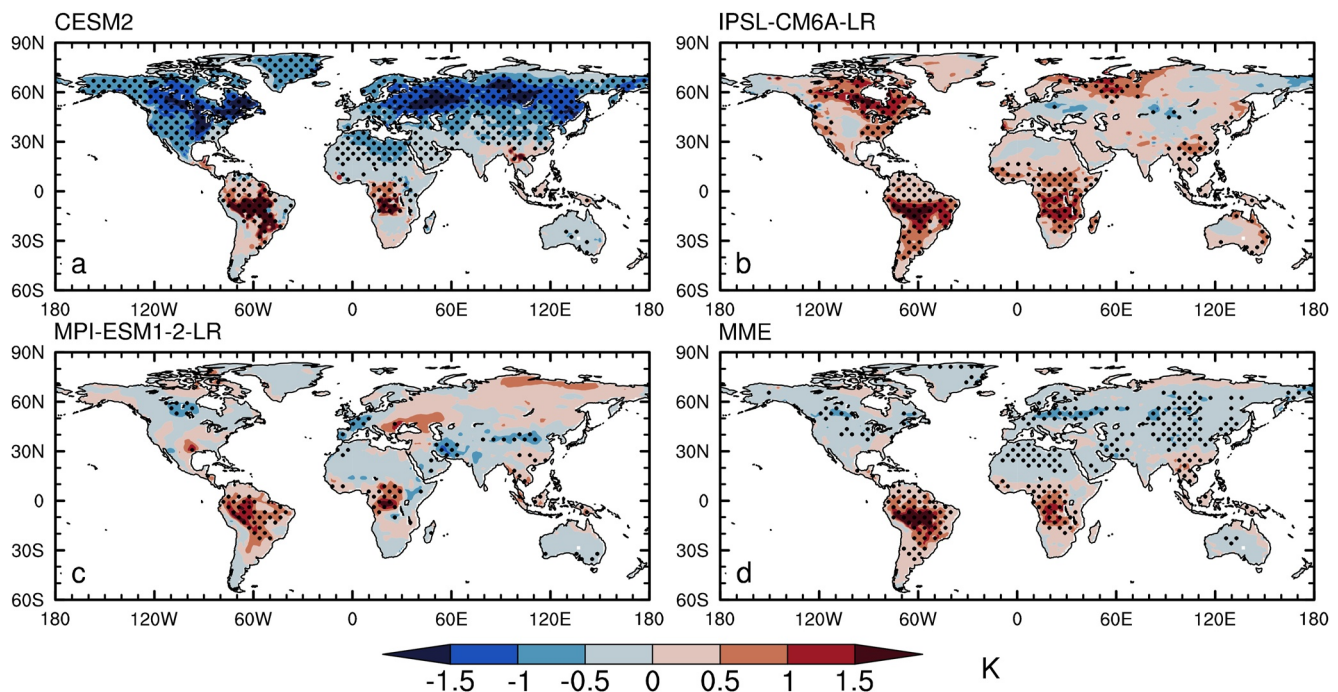


Figure 3. Changes in JJA Ts (K) in response to the idealized deforestation simulations in (a) CESM2, (b) IPSL-CM6A-LR, (c) MPI-ESM1-2-LR, and (d) MME. The changes were computed as the differences between the deforest-globe relative to piControl simulations. The stippling indicates that the differences are statistically significant at the 0.05 level based on a modified Student's *t* test.

these competing processes remains uncertain in model simulations (Boysen et al., 2020; De Noblet-Ducoudré Et Al., 2012; Lejeune et al., 2017; Pitman et al., 2012).

Figure 3 shows the JJA mean Ts changes in responses to deforestation. Tropical deforestation leads to a warming effect in summer, and all models agree on the sign of the temperature changes in South America and Central Africa. CESM2 produces the largest warming in response to deforestation, whereas MPI-ESM1-2-LR exhibits the weakest warming signal in the tropics (Figure 3). It is worth noting that the mean Ts changes due to deforestation are heterogeneous among the models in the temperate and boreal regions and the temperature responses largely depend on the choice of model. For example, CESM2 shows strong cooling in the extratropical regions, while the temperature response in IPSL-CM6A-LR is opposite to CESM2 in both North America and mid-latitudes Eurasia (Figure 3b). In MPI-ESM1-2-LR, the Ts response is weak in the temperate and boreal regions (Figure 3c).

Overall, CMIP6 models agree on the sign of Ts changes due to deforestation in the tropics (e.g., South America and Central Africa), but the Ts changes in response to deforestation are heterogeneous among the models in the temperate and boreal regions.

3.2. Changes in Surface Energy Budget

To further attribute the temperature response to deforestation, we examined the surface energy fluxes in the model simulations. Converting forests to grasses not only influences the radiative processes driven by increased albedo, but also affects the non-radiative effects driven by the changes in available energy partitioning (Bright et al., 2017; Chen et al., 2020; Liu et al., 2021; Rigden & Li, 2017). In general, deforestation-induced albedo increases could lead to a decrease in shortwave radiation absorbed by the surface (cooling effect) over the deforested areas (Figure 2). However, the modeled net shortwave radiation changes in response to deforestation are mixed due to complicated interactions among cloud, precipitation and atmospheric circulation (Duveiller et al., 2021; Laguë & Swann, 2016; Xu et al., 2022). For example, the increase in surface net shortwave radiation in parts of Amazon may result from the decrease in cloud cover (Figure S1 in Supporting Information S1). In addition to shortwave radiation, the net longwave radiation also significantly decreases in the tropics (Figure S2 in Supporting Information S1). The combined shortwave and longwave radiation changes (i.e., net radiation)

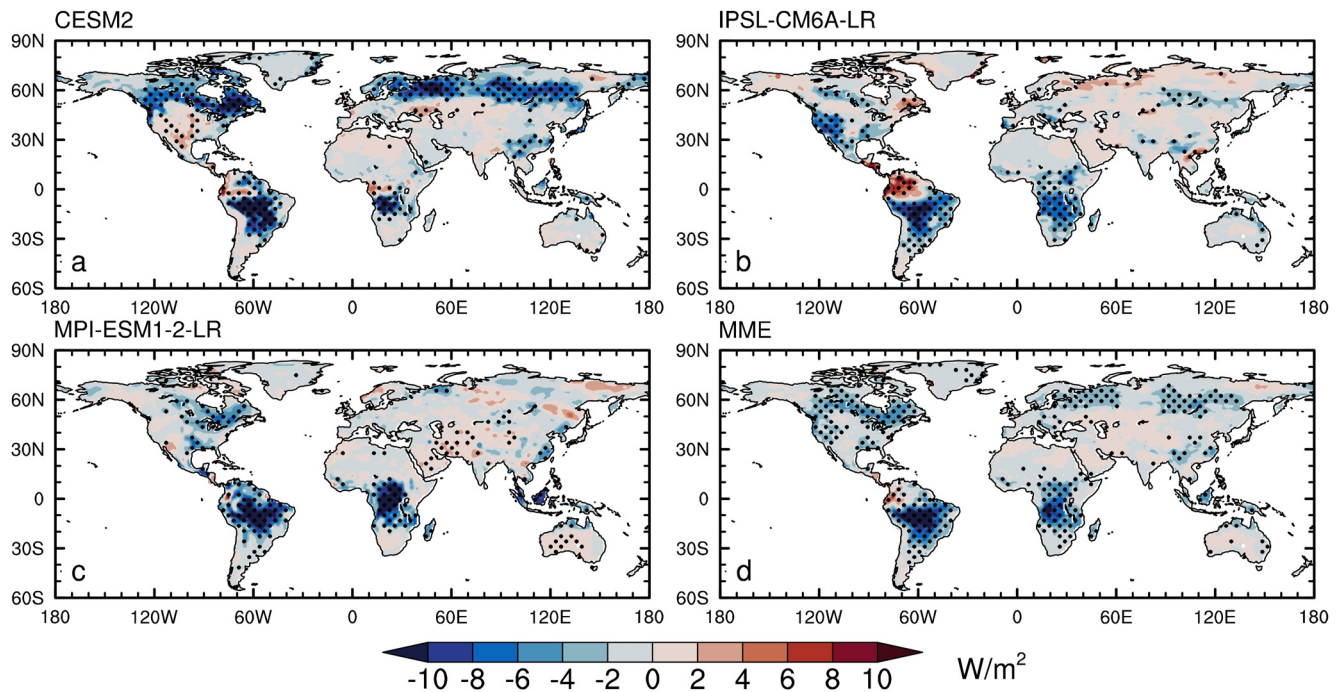


Figure 4. Changes in JJA surface net radiation (W m^{-2}) in response to idealized deforestation simulations in (a) CESM2, (b) IPSL-CM6A-LR, (c) MPI-ESM1-2-LR, and (d) MME. The changes were computed as the differences between the deforest-globe relative to piControl simulations. The stippling indicates that the differences are statistically significant at the 0.05 level based on a modified Student's t test. The negative (positive) net radiation represents less (more) solar radiation absorbed by the surface (i.e., positive in the downward direction).

due to deforestation broadly exhibit a decreasing trend over the deforested areas in the tropics, but diverge in the middle and high latitudes (Figure 4). On the other hand, deforestation also influence regional climate through the non-radiative processes (Figure 5 and Figure S3 in Supporting Information S1). Previous modeling studies have

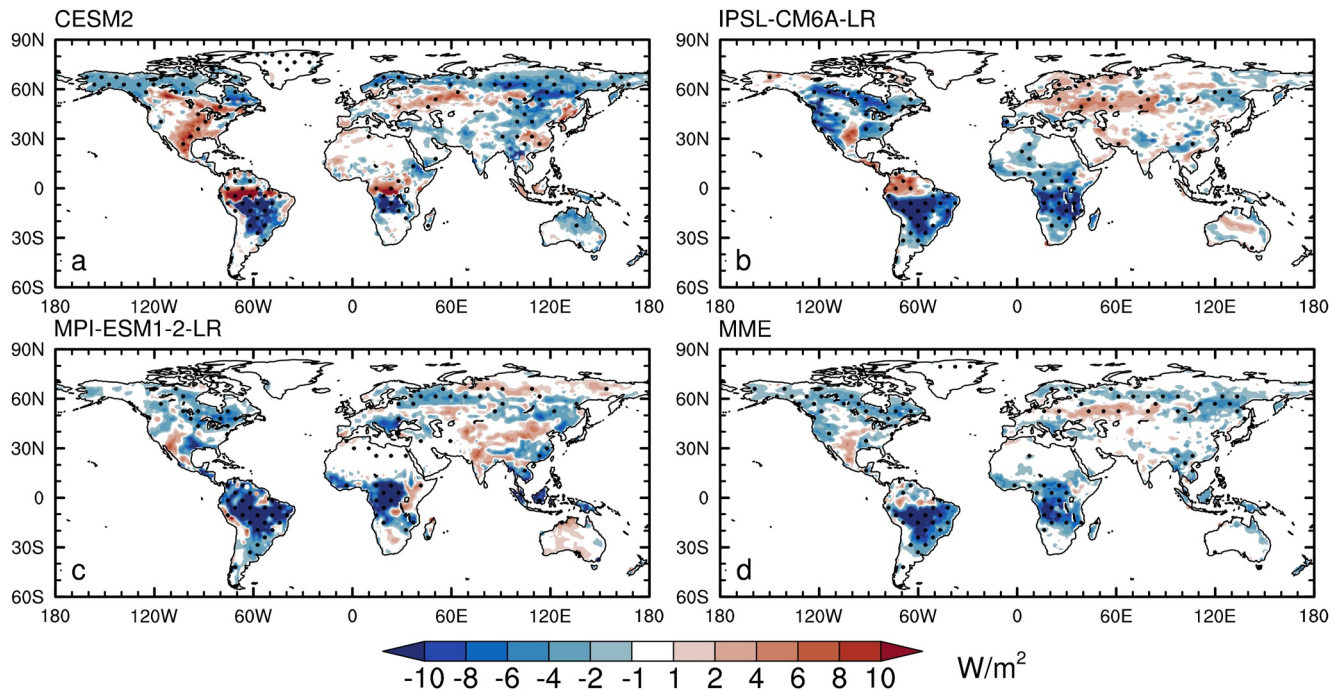


Figure 5. Same as Figure 4, but for the latent heat flux (W m^{-2}). We take the upward direction as positive.

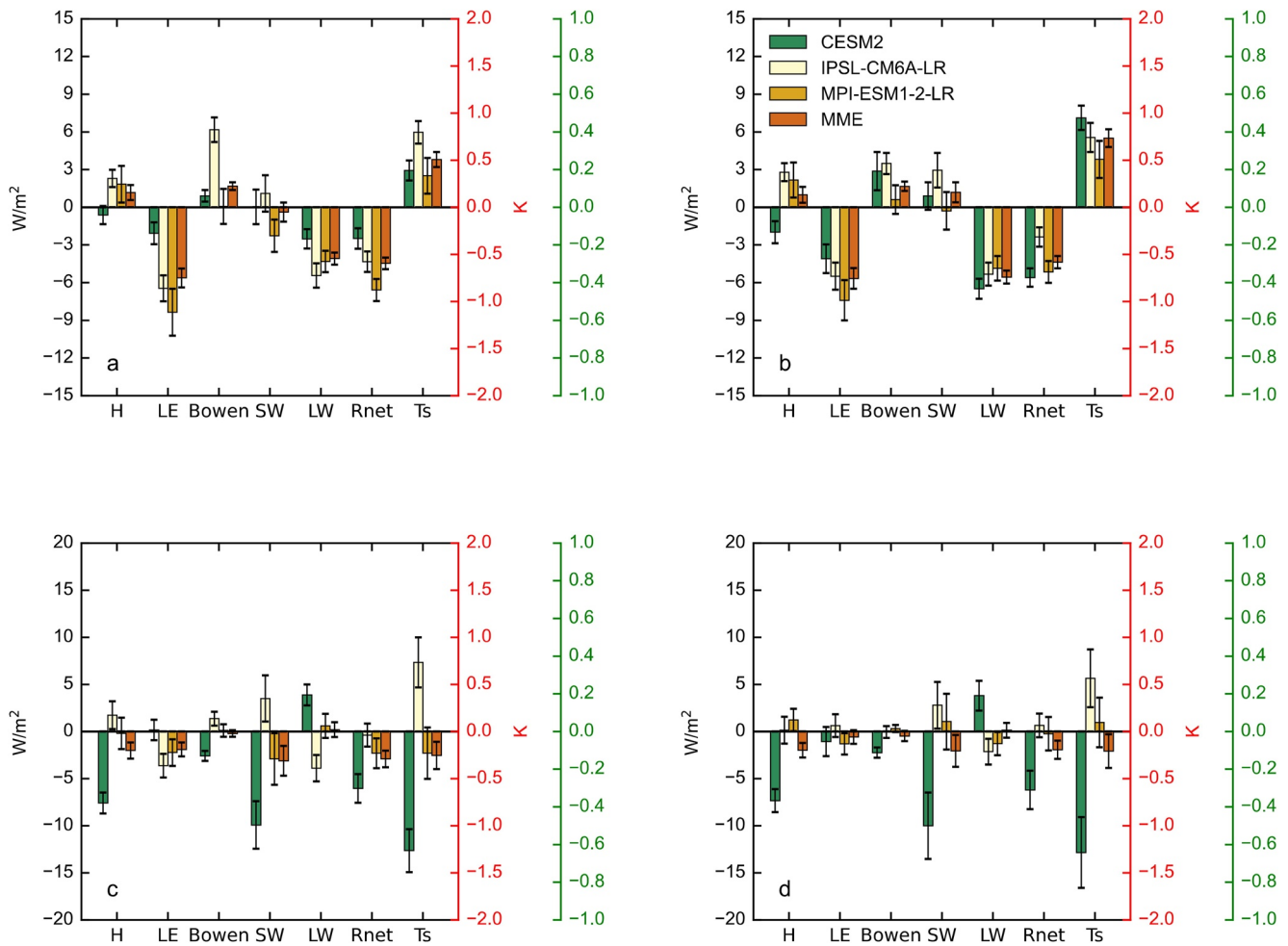


Figure 6. Changes in JJA surface energy budget (black, $W\ m^{-2}$) and T_s (K, units in red) due to deforestation averaged over (a) Central Africa, (b) South America, (c) North America and (d) Eurasia in CESM2, IPSL-CM6A-LR, MPI-ESM1-2-LR, and MME. The surface energy fluxes include sensible heat (H, positive direction is upward), latent heat (LE, positive direction is upward), net shortwave radiation (SW, positive direction is downward), net longwave radiation (LW, positive direction is downward), net radiation (Rnet, positive direction is downward) and Bowen ratio (units in green).

indicated a significant impact of LULCC on the latent heat flux over the regions where vegetation was changed (e.g., De Noblet-Ducoudre et al., 2012; Pitman et al., 2009). The turbulent heat flux (mainly latent heat, positive to the atmosphere) is reduced (Figure S4 in Supporting Information S1), which results in a warming effect in T_s . Note that the increased latent heat flux in north Amazon in IPSL-CM6A-LR and CESM2 is inconsistent with previous studies (Duveiller et al., 2018; Lawrence & Vandecar, 2015). Such discrepancies might be due to the potential problems in the representation of hydrology in land surface models (Cai et al., 2019; Chen & Dirmeyer, 2016; Tafasca et al., 2020).

To examine the regionally aggregated responses to deforestation, we analyzed four regions with the largest deforested areas (Figure 6). In the tropics, the changes in surface energy budget are broadly consistent between Central Africa and South America, where deforestation leads to a decrease in longwave and net radiation absorbed by the surface (Figures 6a and 6b). The magnitude of tropical warming in MPI-ESM1-2-LR is smaller because the warming induced by the turbulent heat fluxes may be offset by significantly albedo-induced cooling (Figure 2). That is, shortwave radiation absorbed by the surface is balanced by the sensible heat, latent heat or longwave radiation. In the mid to high latitudes, the surface net shortwave and longwave radiations in response to deforestation vary among the three models (Figures 6c and 6d). CESM2 shows significant decreased (increased) net shortwave (longwave) radiations in North America and Eurasia, whereas IPSL-CM6A-LR exhibits opposite changes in these two regions. The magnitude of mid-latitude cooling is strongest in CESM2 (Figure 2) because the albedo-induced cooling dominates over the warming effect induced by changes in turbulent heat fluxes (Figures 6c and 6d). These

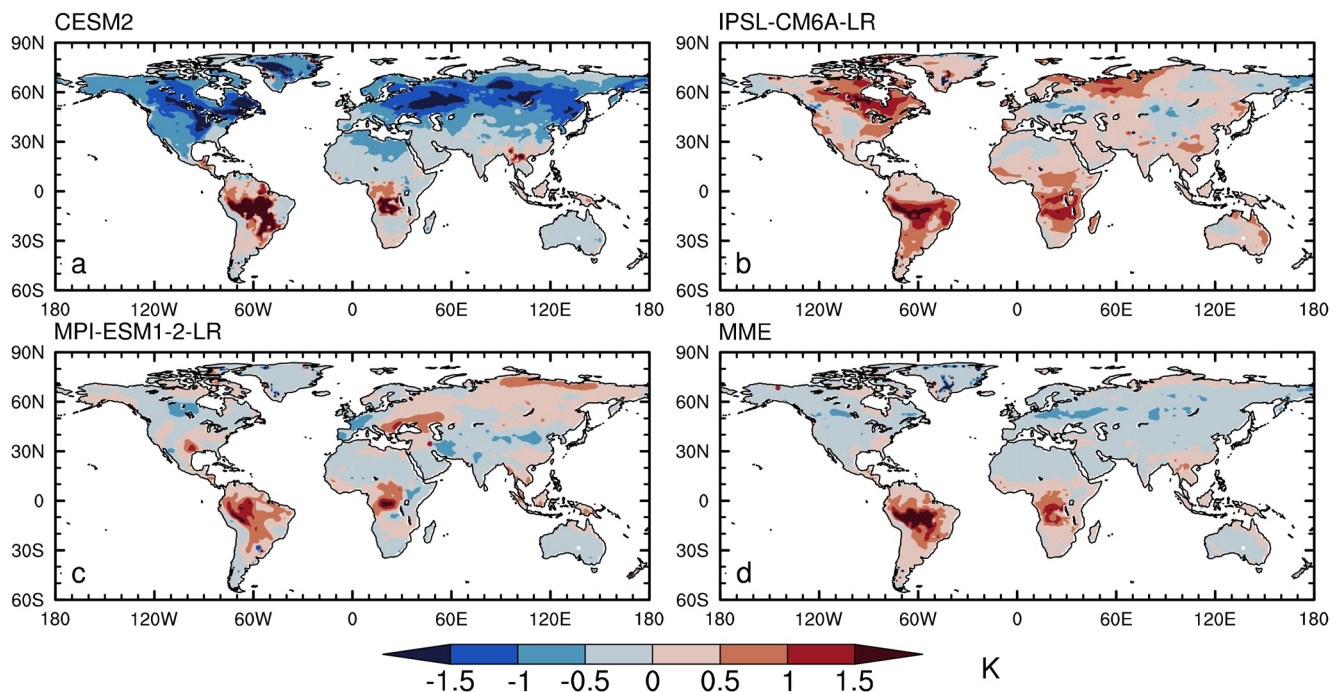


Figure 7. Total changes in JJA Ts (K) in response to deforestation in (a) CESM2, (b) IPSL-CM6A-LR, (c) MPI-ESM1-2-LR, and (d) MME. The total change of Ts is calculated from the revised IBPM (i.e., sum of the contributions of radiative forcing, aerodynamic resistance, Bowen ratio and atmospheric feedbacks).

results suggest that climate models may have a large spread in simulating the energy exchange between the land and the atmosphere and the Bowen ratio (i.e., defined as the ratio of sensible to latent heat fluxes) also shows large differences (e.g., different signs) in the mid to high latitudes. The different Bowen ratios in the model simulations cause the Ts discrepancies through the non-radiative processes (Figure 6). Overall, the energy distribution changes show different responses in different models, and the simulated energy fluxes in the mid to high latitudes have a strong model dependency.

3.3. Surface Temperature Change Decomposition

To investigate the possible mechanism for deforestation-driven temperature changes, the revised IBPM (i.e., Equation 9) is used to separate the biophysical effects of deforestation into four components (e.g., radiative forcing, aerodynamic resistance, Bowen ratio, and atmospheric feedbacks). Before examining the individual biophysical factors, we need to know whether the decomposed temperature metric can realistically capture the spatial pattern of Ts in models. In general, the revised IBPM well captures the spatial pattern of the model's actual Ts change (Figure 7). Figure 7d shows that deforestation decreases Ts in the middle and high latitudes, but increases Ts in the tropics based on the decomposed method, which shows agreement with the simulated Ts (Figure 3d). Therefore, the revised IBPM can be used to investigate the biophysical effects of deforestation (Chen & Dirmeyer, 2016; Liao et al., 2018).

The radiative and non-radiative (e.g., radiative forcing, Bowen ratio, aerodynamic resistance) effects of Ts due to deforestation are shown in Figure 8, which represent the local biophysical impacts due to the changes in surface physical properties and surface energy balance. Our results show that changes in the aerodynamic resistance dominate the surface temperature response to local biophysical effect of deforestation. The Ts changes associated with radiative forcing and Bowen ratio is relatively weak (Figure 8). CESM2 and IPSL-CM6A-LR show a strong local warming over the deforested regions due to aerodynamic resistance changes during boreal summer, in particular in the tropics (Figures 8b and 8e). However, there exist some regional differences in MPI-ESM1-2-LR (Figure 8h). Based on the multimodel ensemble results, it can be found that deforestation contributes to the local warming across the global regions during the boreal summer and aerodynamic resistance dominates the local biophysical impact of deforestation (Figure 8).

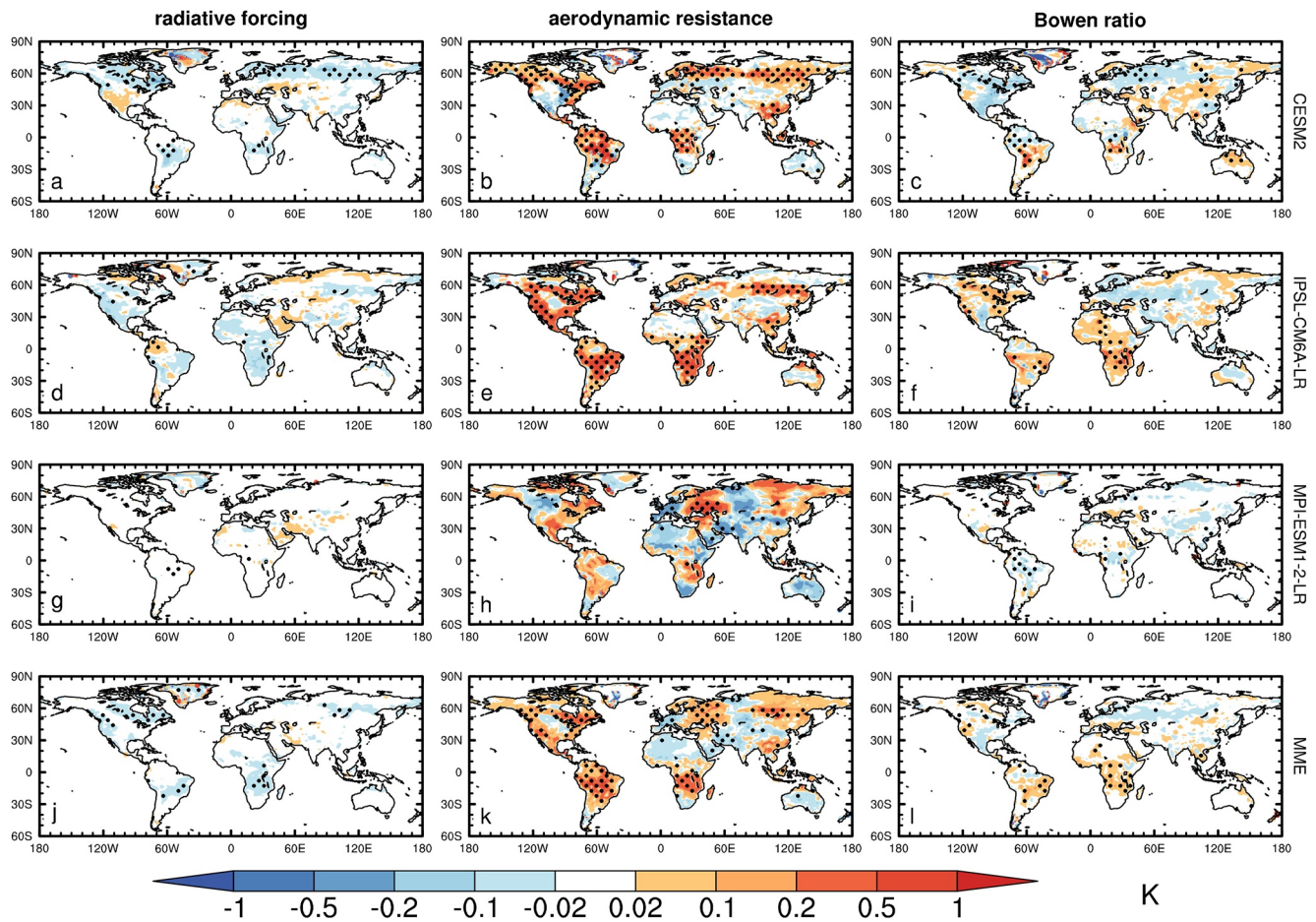


Figure 8. Changes in JJA Ts (K) in response to deforestation in (a–c) CESM2, (d–f) IPSL-CM6A-LR, (g–i) MPI-ESM1-2-LR, and (j–l) MME. The left column shows the radiative forcing effect associated with albedo change, the middle column shows the aerodynamic resistance effect, and the right column shows the Bowen ratio effect. The stippling indicates that the differences are statistically significant at the 0.05 level based on a modified Student's *t* test.

To reveal the possible mechanisms behind the heterogeneous modeled temperature responses to deforestation, we also examined individual biophysical factors over four deforested regions (Figure 9). In general, aerodynamic resistance change associated with local warming is more important in determining the Ts changes than radiative forcing and Bowen ratio, not only over the deforested areas in the tropics, but also in the mid-latitudes (Figure 8). This explains why most climate models exhibit a local warming effect across the global deforested regions. Our results are consistent with recent observational and modeling studies, which suggest that non-radiative processes (e.g., aerodynamic resistance) dominate the local biophysical effects (Bright et al., 2017; Chen & Dirmeyer, 2016; Duveiller et al., 2018; Winckler, Reick, Bright, et al., 2019). Chen et al. (2020) also examined the biophysical impact of LAI changes and found that the aerodynamic resistance has the dominant role. However, these findings are inconsistent with the earlier view that albedo-induced changes from deforestation dominate the widespread cooling in the extratropical areas in models (Betts, 2000; Pongratz et al., 2021). For example, albedo-induced warming due to boreal afforestation may be stronger than CO₂-induced cooling (Betts, 2000). Indeed, the albedo effect is more important in model simulations when total (local and non-local) effects are considered (Boysen et al., 2020; Winckler, Lejeune, Luysaert, et al., 2019), although it is difficult to attribute the non-local albedo effect at individual regions. The aerodynamic resistance effect dominates the biophysical feedback over the deforested regions when only the local effect (e.g., ignoring the non-local atmospheric feedbacks) is taken into account, while albedo and the Bowen ratio play a minor role.

In addition to the local effects, the atmospheric feedbacks from deforestation are seen not only over the deforested regions but also over remote locations. We used the Ta changes to represent atmospheric feedbacks due to the changes in heat and moisture advection and atmospheric circulation. The Ta signals are similar in the

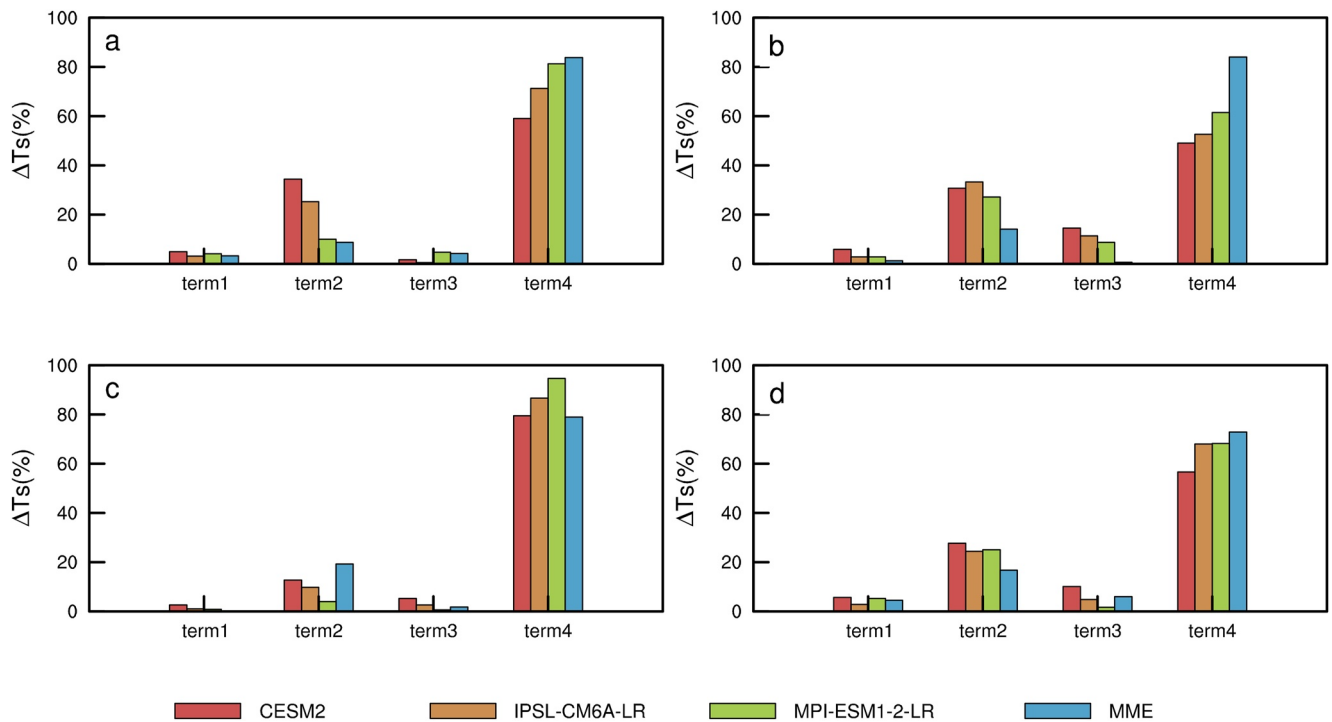


Figure 9. Contribution (%) of radiative forcing (term1), aerodynamic resistance (term2), Bowen ratio (term3), and atmospheric feedbacks (term4) effects to total changes of Ts over four deforested regions in CESM2, IPSL-CM6A-LR, MPI-ESM1-2-LR, and MME. The regions include: (a) Central Africa, (b) South America, (c) North America, and (d) Eurasia.

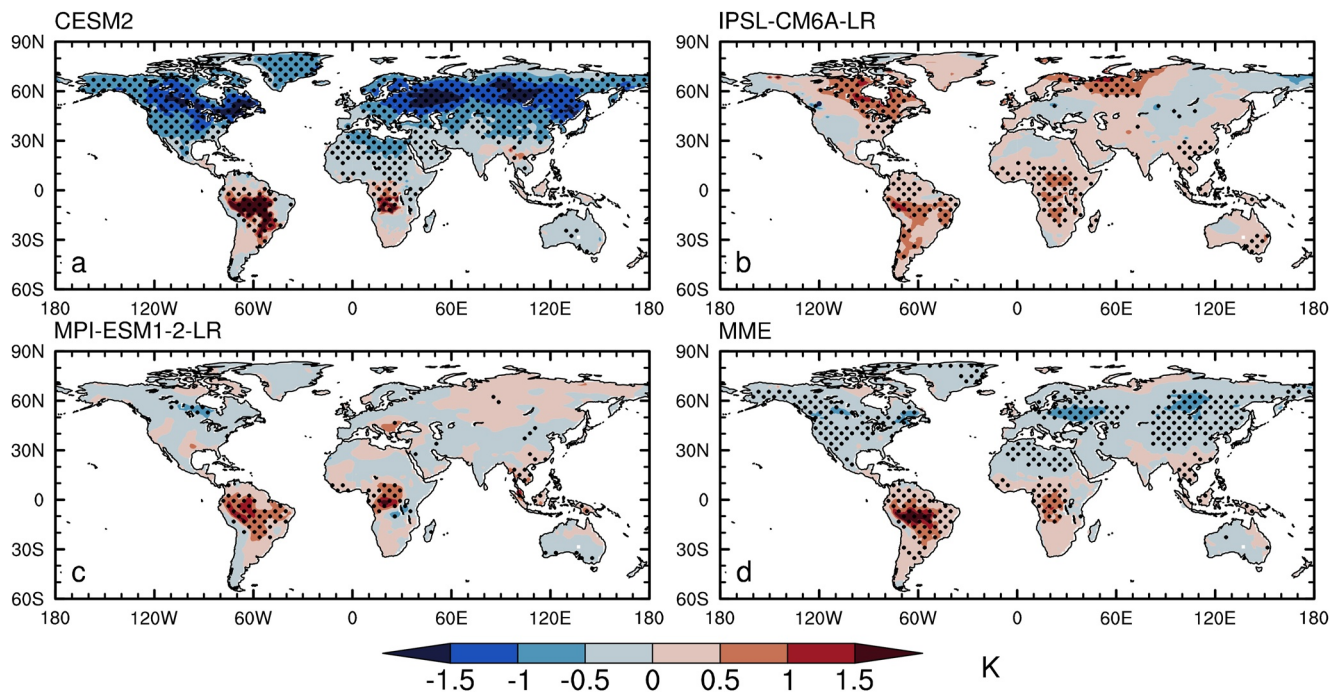


Figure 10. Changes in JJA Ta (K) in response to the idealized deforestation simulations in (a) CESM2, (b) IPSL-CM6A-LR, (c) MPI-ESM1-2-LR, and (d) MME, which represents the atmospheric feedbacks. The changes were computed as the differences between the deforest-globe relative to piControl simulations. The stippling indicates that the differences are statistically significant at the 0.05 level based on a modified Student's *t* test.

tropics among the three models, but exhibits significant difference in the middle and high latitudes (Figure 10). For example, CESM2 shows a strong cooling in the extratropical regions, but a strong warming in the tropics (Figure 10a). That is, deforestation-induced local warming (e.g., due to aerodynamic resistance effect) is amplified by a strong warming due to atmospheric feedbacks in the tropics in CESM2. IPSL-CM6A-LR shows mixed signals over Eurasia, with a cooling over the parts of northeast Asia and a strong warming over North America and northern western-central Russia (Figure 10b). MPI-ESM1-2-LR shows weak and contrast changes in the mid-latitudes, with a cooling over North America and a strong warming over central Russia (Figure 10c).

Note that T_s changes indirectly via perturbations in T_a . For example, T_a contributes to the opposite changes between the extratropical regions and tropics in CESM2 (Figure 10a). We infer that the atmospheric feedbacks in the tropics is likely due to decreased evapotranspirative cooling and increased incoming radiations resulting from deforestation-induced changes in cloud cover and water vapor. Our study also highlights the importance of non-local effect from atmospheric feedbacks in determining the influence of deforestation on T_s in the extratropical areas (Figures 9 and 10), as the T_a changes are also seen over remote locations. These results are consistent with previous findings using idealized deforestation and CMIP5-LUCID simulations, which suggest that changes in atmospheric feedbacks dominate the other biophysical factors (Figure 9, Devaraju et al., 2018). To further this finding, we also examined the vertical profile of regional mean tropospheric temperatures averaged over four deforested regions (Figure 11). Evidently, the deforestation impacts are not limited to T_s and T_a at 2-m, and LULCC can lead to significant changes in the entire tropospheric air temperatures in model simulations (e.g., Zhang et al., 2016). In addition, such impacts on the troposphere are much stronger and deeper in the mid-latitudes than the tropics, particularly in CESM2 (Figure 11). Our results show that CESM2 and IPSL-CM6A-LR models show opposite changes in tropospheric temperatures due to deforestation (Figure 11). In CESM2, the significantly decreases in the absorbed solar radiation and sensible heat flux and associated cooling of the air (e.g., horizontal temperature advection) play a dominant role in the indirect feedback in the extratropical regions (Figures 6, 9, and 10). In contrast, the tropospheric warming occurs in IPSL-CM6A-LR (Figure 11), which can be attributed to the increase in the absorbed solar radiation (Figure 6).

To explore the possible biophysical effects for the inter-model spread, we also examined the contributions of different biophysical effects over the four deforested regions (Figure 9). All models exhibit larger atmospheric feedbacks changes than the local effects (Figure 9). Note that the local effects rarely affect the areas away from the deforested regions (Chen & Dirmeyer, 2016; Lee et al., 2011). Thus, their contribution to the non-local signal or atmospheric circulation is very small. Previous modeling studies have indicated that climate models exhibit divergent changes in the sign and magnitude of temperatures in response to deforestation in particular in the mid-latitudes (Boisier et al., 2012; Davin et al., 2020; De Noblet-Ducoudré et al., 2012; Lejeune et al., 2017; Pitman et al., 2009). Our results further suggest that much of the discrepancies may be due to the different atmospheric feedbacks simulated in the mid-latitudes in climate models, as a large proportion of T_s changes can be explained by the atmospheric feedbacks (Figure 9). The partitioning of these biophysical contributions can explain the inter-model spread in CMIP6 models. It is worth noting that MPI-ESM1-2-LR exhibits contrasting changes in the sign and magnitudes of tropospheric temperatures over Eurasia and North America (Figure 11). This explains why the total T_s responses due to deforestation are less significant in the extratropical regions (Figure 3c). The non-local effects cancel each other out (Figure 10).

4. Discussion

In this study, we adopted a revised decomposition method of intrinsic biophysical mechanisms to separate the biophysical effects of deforestation into different components (e.g., radiative forcing, aerodynamic resistance, Bowen ratio and atmospheric feedbacks; Chen & Dirmeyer, 2016; Lee et al., 2011; Liao et al., 2018). The method can be used to quantify the relative importance of individual biophysical factors that contribute to T_s change in CMIP6 models, but does have some limitations. First, we linearized the surface energy budget equation using a Taylor series expansion to retain only the first-order terms, and did not consider non-linear interactions among these terms. For example, Bowen ratio may be changed by sensible and latent heat fluxes due to radiative forcing and atmospheric feedbacks associated with variations in circulation and advection of heat and moisture. Aerodynamics resistance depends on the Monin-Obukhov length which is a function of atmospheric stability and the Monin-Obukhov theory relates to surface vertical turbulent fluxes of momentum, sensible heat, and water vapor with profiles of wind speed, potential temperature, and humidity. Furthermore, there also exists uncertainties

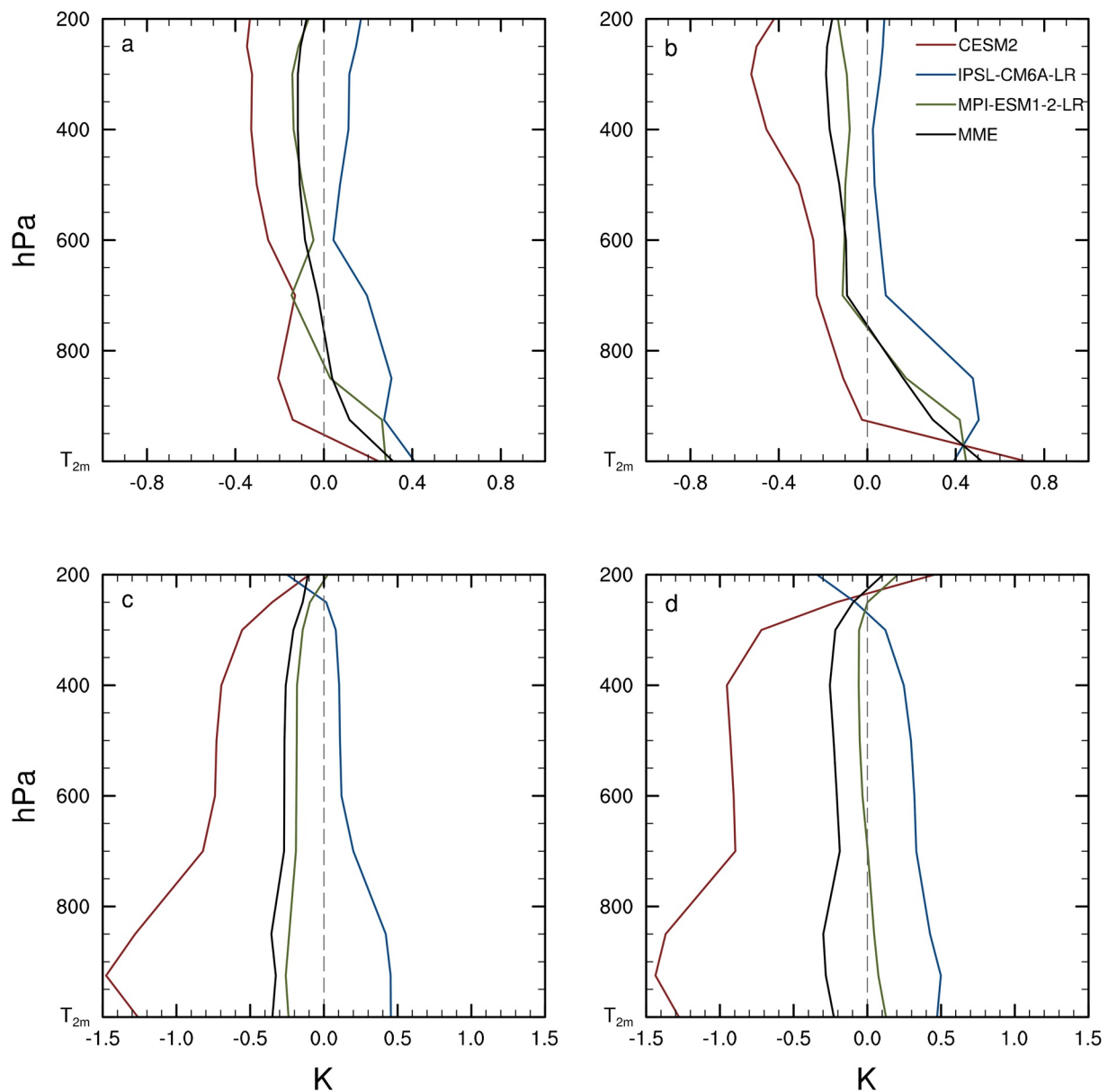


Figure 11. The vertical profile of regional mean atmospheric air temperature and 2-m temperature (T_{2m}) averaged over (a) Central Africa, (b) South America, (c) North America, and (d) Eurasia due to deforestation during boreal summer. The changes were computed as the differences between the deforest-globe relative to piControl simulations.

in estimating the aerodynamic resistance (depending on T_s as well), as aerodynamic resistance is a non-linear function of T_s in models (see Equation 2). Thus, one needs to interpret our results with these constraints in mind. Nevertheless, the higher-order interactions between these biophysical effects are likely to be small and could be ignored (Devaraju et al., 2018; Liao et al., 2018). This is confirmed by the reproduction of modeled T_s by the first four terms of decomposed T_s in Equation 9 (Figure 7), indicating that the first-order Taylor series expansion suffices for obtaining an analytical form of surface temperature (Devaraju et al., 2018; Liao et al., 2018).

Second, we used T_a change to represent atmospheric feedbacks from deforestation (Chen & Dirmeyer, 2016; Liao et al., 2018), which may affect the local and remote areas through advection of heat and moisture and by changes in atmospheric circulation (Winckler, Lejeune, et al., 2019). For example, temperate deforestation can affect cloud, precipitation and large scale atmospheric circulation in regions far away from the deforested regions through atmospheric teleconnections (Devaraju et al., 2015; Laguë & Swann, 2016). However, the indirect

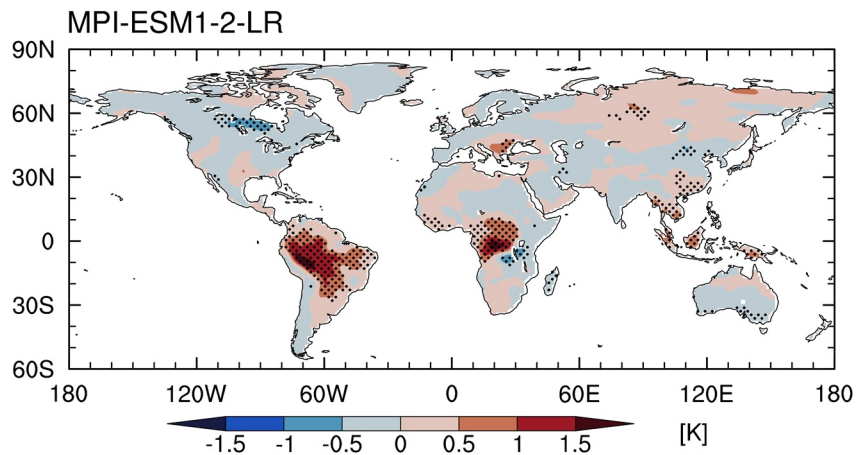


Figure 12. Changes in JJA temperature at the lowest atmospheric model level in response to the idealized deforestation simulations in MPI-ESM1-2-LR model. The changes were computed as the differences between the deforest-globe relative to piControl simulations. The stippling indicates that the differences are statistically significant at the 0.05 level based on a modified Student's *t* test.

feedbacks (e.g., interactions between water vapor, clouds and atmospheric circulation) are probably not fully captured and quantified by our decomposition method, although this method provided insight into the causes of inter-model spread and uncertainties of deforestation-driven changes. Quantifying these impacts is thus a daunting challenge, in particular related to tropospheric temperatures. The air temperature feedback in the context of large scale deforestation or LULCC needs to be treated with caution in the future. Furthermore, if we focus on the short-term simulations or use the flux tower observations, the energy imbalances or the contribution of ground heat flux should not be ignored (Chen & Dirmeyer, 2016; Juang et al., 2007; Luyssaert et al., 2014).

Our results suggested that the temperature and energy fluxes outside the deforested areas also show significant changes in CMIP6 models. That is, significant atmospheric circulations may be triggered from deforestations. However, the non-local signals must be treated with caution due to model uncertainties and lack of a sufficiently large ensemble. First, not all models agree on the sign of regional temperature changes due to atmospheric feedbacks of deforestation in the middle and high latitudes. The models not only continue to show significant differences in the partitioning of available turbulent heat into sensible and latent fluxes (e.g., Bowen ratio), but exhibit large differences in partitioning among different biophysical factors. The sign and strength of biophysical effects is highly dependent on the indirect influences of atmospheric feedbacks in the model simulations. Second, the extratropical responses across the individual runs due to model internal variability also show considerable intra-ensemble spread (not shown). Thus, further efforts using multiple models with multiple realizations to minimize the model internal variability or “noise” are needed, as a limited number of realizations cannot give a robustness estimate of climate responses due to deforestation. At the time of this study, 12 CMIP6 models have provided the outputs of idealized deforestation experiments, but only three models (used in this study) have multiple realizations. Furthermore, climate models can not only capture the total changes over the deforested regions (i.e., local effects), but simulate the non-local or remote effects that observationally based methods probably cannot identify. Some approaches were developed to separate local and non-local effects (Chen & Dirmeyer, 2020; Malyshev et al., 2015; Winckler et al., 2017). However, the models may have large uncertainties in simulating the large scale atmospheric feedback. It is therefore necessary to quantify the local response over the deforested regions and the non-local signals outside the deforested areas in the future. This could help advance our understanding of the biophysical effects on global climate and is beneficial for policy makers to consider the biophysical effects of LULCC.

Interestingly, the spatial pattern of T_a responses is similar to the T_s changes due to deforestation, although the magnitudes of the variations in T_a is smaller than that of the T_s (Figures 3 and 9). Note that the near-surface T_a , as a diagnostic quantity, is dependent on T_s and air temperature at the lowest atmospheric level in climate models (Breil et al., 2020; Winckler, Reick, Luyssaert, et al., 2019). There are complex interactions between surface and near-surface temperatures and planetary boundary layer (PBL) processes in the fully coupled land-atmosphere system (Zhou, 2021). We also examined the temperature variations due to the deforestation at the lowest

atmospheric model level (Figure 12). Among the models, only MPI-ESM1-2-LR provides the global temperature data at the lowest atmospheric layer. The spatial pattern of the temperature responses is very similar among the lowest atmospheric model level, near-surface and at the surface (Figures 3, 10 and 12). Jiang et al. (2021) also suggested that deforestation-induced warming signal for surface air is weaker than for ground and vegetation. In general, forests, which have larger aerodynamic roughness, dissipate sensible heat more efficiently to the atmospheric boundary layer (Lee et al., 2011; Rotenberg & Yakir, 2010). That is, reduced surface roughness due to deforestation could suppress the sensible heat flux (Jiang et al., 2021). These results indicate that the surface temperature and air temperature can be less coupled (e.g., Jiang et al., 2021). Most observational studies compared temperature differences between forest and nearby open land, which reflect primarily the differences in ground temperature (as opposed to air temperature), and thus cannot capture this atmospheric feedback that is important for the simulated T_a response in the models (e.g., Chen & Dirmeyer, 2020; Hirsch et al., 2014).

It is well known that climate models have deficiencies in various parameterization schemes and thus could result in biased deforestation effects (e.g., soil evaporation, snow-albedo feedback or partitioning of available energy into latent and sensible heat fluxes) in land surface models (Cai et al., 2019; Chen et al., 2018; Li et al., 2018; Zhou et al., 2003). For example, the T_s change due to albedo reduction is the result of two counteracting processes (e.g., changes in surface net radiation and the corresponding response of turbulent fluxes) whose net effect may depend on subtle details of the model formulation. The deforestation-induced change in surface albedo in the MPI-ESM, for instance, is lower than that in observations and also on the lower end of a range of climate models (Boisier et al., 2013). And CMIP5 models generally overestimated the seasonal cycle of albedo, which is related to seasonal variations in snow cover fraction and albedo contrast (Li, Wang, et al., 2016). Meier et al. (2022) suggested that the revisions of roughness in the land component of the CESM alter the local T_s response to a conversion of vegetation to bare land, which could be relevant for the simulated biophysical effect of desertification. The updated parameterizations of roughness lengths could also reduce the mean biases of the simulated daytime surface temperature in land surface models (Huang et al., 2016). However, each of the GCMs uses different land-surface parameterizations/models and a detailed analysis of different parameterization schemes is beyond the scope of this study. Further investigation using various improved land-surface parameterizations will corroborate and refine our diagnostic results.

5. Conclusions

In this study, we analyzed CMIP6-LUMIP multimodel simulations from three models (i.e., CESM2, IPSL-CM6A-LR, and MPI-ESM1-2-LR) to show that the biophysical effects of deforestation have a strong latitudinal dependence during boreal summer. CMIP6 models agree on the sign of the temperature changes due to deforestation in the tropics (e.g., South America and Central Africa). In contrast, the temperature changes in response to deforestation are heterogeneous among the models in the temperate and boreal regions (e.g., North America and Eurasia). In addition to the temperature changes, the surface net shortwave and longwave radiations and Bowen ratio in response to deforestation vary in models in the middle and high latitudes. CESM2 shows significant decreased (increased) net shortwave (longwave) radiations in North America and Eurasia, whereas IPSL-CM6A-LR exhibits opposite changes in these two regions. Our results suggest that climate models have a large spread in simulating the energy exchange between the land and the atmosphere, in line with previous studies using CMIP5-LUCID simulations (Boisier et al., 2012; De Noblet-Ducoudré et al., 2012; Lejeune et al., 2017; Pitman et al., 2009).

We used a revised intrinsic biophysical mechanism approach to separate the biophysical effects of deforestation into different components (i.e., radiative forcing, aerodynamic resistance, Bowen ratio and atmospheric feedbacks). CMIP6 models show local warming due to local biophysical effects in response to a local perturbation in radiative forcing, aerodynamic resistance and Bowen ratio. Aerodynamic resistance is the dominant factor contributing to the local warming when compared with radiative forcing and Bowen ratio. For the atmospheric feedbacks, climate models show consistent changes in the tropics, but exhibit significant differences in the middle and high latitudes. Air temperature feedbacks are seen not only over the deforested regions but also over remote locations. Models exhibit a dominant but model-dependent contribution of T_a effects on T_s changes and much of the modeled discrepancies in the middle and high latitudes are likely due to the differences in simulating these effects. Our study highlights the importance of atmospheric feedbacks (e.g., feedback effects of cloud, water vapor, soil moisture and atmospheric circulation). These results provide a first-order estimate of different

biophysical factors in determining the surface temperature changes following deforestation and help improve our understanding of responses to deforestation in CMIP6 models.

Data Availability Statement

The CMIP6-LUMIP data sets (Lawrence et al., 2016) used in this study are available at <https://esgf-node.llnl.gov/search/cmip6/>.

Acknowledgments

This work was supported by the National Key R&D Program of China (2022YFF0801601), the National Natural Science Foundation of China (42075022) and the National Natural Science Foundation of Jiangsu Province (BK20200096). L. Zhou was supported by the US National Science Foundation (AGS-1952745). M. Yu was supported by the National Natural Science Foundation of China (42075115). X. Li was supported by the National Natural Science Foundation of China (41905080). We thank Dr. Nan Wei from Sun Yat-sen University for valuable discussions and comments. We acknowledge the World Climate Research Programme, which, through its Working Group on Coupled Modelling, coordinated and promoted CMIP6. We thank the climate modeling groups for producing and making available their model output, the Earth System Grid Federation (ESGF) for archiving the data and providing access, and the multiple funding agencies who support CMIP6 and ESGF.

References

- Alkama, R., & Cescatti, A. (2016). Biophysical climate impacts of recent changes in global forest cover. *Science*, 351(6273), 600–604. <https://doi.org/10.1126/science.aac8083>
- Bala, G., Caldeira, K., Wickert, M., Phillips, T. J., Lobell, D. B., Delire, C., & Mirin, A. (2007). Combined climate and carbon-cycle effects of large-scale deforestation. *Proceedings of the National Academy of Sciences of the United States of America*, 104(16), 6550–6555. <https://doi.org/10.1073/pnas.0608998104>
- Bathiany, S., Claussen, M., Brovkin, V., Raddatz, T., & Gayler, V. (2010). Combined biogeophysical and biogeochemical effects of large-scale forest cover changes in the MPI Earth system model. *Biogeosciences*, 7(5), 1383–1399. <https://doi.org/10.5194/bg-7-1383-2010>
- Betts, R. A. (2000). Offset of the potential carbon sink from boreal forestation by decreases in surface albedo. *Nature*, 408(6809), 187–190. <https://doi.org/10.1038/35041545>
- Betts, R. A., Falloon, P. D., Goldewijk, K. K., & Ramankutty, N. (2007). Biogeophysical effects of land use on climate: Model simulations of radiative forcing and large-scale temperature change. *Agricultural and Forest Meteorology*, 142(2–4), 216–233. <https://doi.org/10.1016/j.agrformet.2006.08.021>
- Boisier, J. P., De Noblet-Ducoudré, N., & Ciais, P. (2013). Inferring past land use-induced changes in surface albedo from satellite observations: A useful tool to evaluate model simulations. *Biogeosciences*, 10(3), 1501–1516. <https://doi.org/10.5194/bg-10-1501-2013>
- Boisier, J. P., De Noblet-Ducoudré, N., Pitman, A. J., Cruz, F. T., Delire, C., Van den Hurk, B. J. J. M., et al. (2012). Attributing the impacts of land-cover changes in temperate regions on surface temperature and heat fluxes to specific causes: Results from the first LUCID set of simulations. *Journal of Geophysical Research*, 117, D12116. <https://doi.org/10.1029/2011JD017106>
- Bonan, G. B. (2008). Forests and climate change: Forcings, feedbacks, and the climate benefits of forests. *Science*, 320(5882), 1444–1449. <https://doi.org/10.1126/science.1155121>
- Bonan, G. B. (2016). Forests, climate, and public policy: A 500-year interdisciplinary odyssey. *Annual Review of Ecology, Evolution, and Systematics*, 47(1), 97–121. <https://doi.org/10.1146/annurev-ecolsys-121415-032359>
- Boucher, O., Servonnat, J., Albright, A. L., Aumont, O., Balkanski, Y., Bastrikov, V., et al. (2020). Presentation and evaluation of the IPSL-CM6A-LR climate model. *Journal of Advances in Modeling Earth Systems*, 12(7), e2019MS002010. <https://doi.org/10.1029/2019MS002010>
- Boysen, L. R., Brovkin, V., Pongratz, J., Lawrence, D. M., Lawrence, P., Vuichard, N., et al. (2020). Global climate response to idealized deforestation in CMIP6 models. *Biogeosciences*, 17(22), 5615–5638. <https://doi.org/10.5194/bg-17-5615-2020>
- Breil, M., Davin, E. L., & Rechid, D. (2021). What determines the sign of the evapotranspiration response to afforestation in European summer? *Biogeosciences*, 18(4), 1499–1510. <https://doi.org/10.5194/bg-18-1499-2021>
- Breil, M., Rechid, D., Davin, E. L., De Noblet-Ducoudré, N., Katragkou, E., Cardoso, R. M., et al. (2020). The opposing effects of reforestation and afforestation on the diurnal temperature cycle at the surface and in the lowest atmospheric model level in the European summer. *Journal of Climate*, 33(21), 9159–9179. <https://doi.org/10.1175/JCLI-D-19-0624.1>
- Bright, R. M., Davin, E., O'Halloran, T., Pongratz, J., Zhao, K., & Cescatti, A. (2017). Local temperature response to land cover and management change driven by non-radiative processes. *Nature Climate Change*, 7(4), 296–302. <https://doi.org/10.1038/nclimate3250>
- Burakowski, E., Tawfik, A., Ouimette, A., Lepine, L., Novick, K., Ollinger, S., et al. (2018). The role of surface roughness, albedo, and Bowen ratio on ecosystem energy balance in the Eastern United States. *Agricultural and Forest Meteorology*, 249, 367–376. <https://doi.org/10.1016/j.agrformet.2017.11.030>
- Cai, X., Riley, W. J., Zhu, Q., Tang, J., Zeng, Z., Bisht, G., & Randerson, J. T. (2019). Improving representation of deforestation effects on evapotranspiration in the E3SM land model. *Journal of Advances in Modeling Earth Systems*, 11(8), 2412–2427. <https://doi.org/10.1029/2018MS001551>
- Chen, C., Li, D., Li, Y., Piao, S., Wang, X., Huang, M., et al. (2020). Biophysical impacts of Earth greening largely controlled by aerodynamic resistance. *Science Advances*, 6(47), eabb1981. <https://doi.org/10.1126/sciadv.abb1981>
- Chen, L., & Dirmeyer, P. A. (2016). Adapting observationally based metrics of biogeophysical feedbacks from land cover/land use change to climate modeling. *Environmental Research Letters*, 11(3), 034002. <https://doi.org/10.1088/1748-9326/11/3/034002>
- Chen, L., & Dirmeyer, P. A. (2020). Reconciling the disagreement between observed and simulated temperature responses to deforestation. *Nature Communications*, 11(1), 202. <https://doi.org/10.1038/s41467-019-14017-0>
- Chen, L., Dirmeyer, P. A., Guo, Z., & Schultz, N. M. (2018). Pairing FLUXNET sites to validate model representations of land-use/land-cover change. *Hydrology and Earth System Sciences*, 22(1), 111–125. <https://doi.org/10.5194/hess-22-111-2018>
- Claussen, M., Brovkin, V., & Ganopolski, A. (2001). Biogeophysical versus biogeochemical feedbacks of large-scale land cover change. *Geophysical Research Letters*, 28(6), 1011–1014. <https://doi.org/10.1029/2000GL012471>
- Danabasoglu, G., Lamarque, J.-F., Bacmeister, J., Bailey, D. A., DuVivier, A. K., Edwards, J., et al. (2020). The community Earth system model version 2 (CESM2). *Journal of Advances in Modeling Earth Systems*, 12, e2019MS001916. <https://doi.org/10.1029/2019MS001916>
- Davin, E. L., & De Noblet-Ducoudré, N. (2010). Climatic impact of global-scale deforestation: Radiative versus nonradiative processes. *Journal of Climate*, 23(1), 97–112. <https://doi.org/10.1175/2009JCLI13102.1>
- Davin, E. L., Rechid, D., Breil, M., Cardoso, R. M., Coppola, E., Hoffmann, P., et al. (2020). Biogeophysical impacts of forestation in Europe: First results from the LUCAS (land Use and climate across scales) regional climate model intercomparison. *Earth System Dynamics*, 11(1), 183–200. <https://doi.org/10.5194/esd-11-183-2020>
- De Noblet-Ducoudré, N., Boisier, J., Pitman, A., Bonan, G. B., Brovkin, V., Cruz, F., et al. (2012). Determining robust impacts of land-use-induced land cover changes on surface climate over North America and Eurasia: Results from the first set of LUCID experiments. *Journal of Climate*, 25(9), 3261–3281. <https://doi.org/10.1175/JCLI-D-11-00338.1>
- Devaraju, N., Bala, G., & Modak, A. (2015). Effects of large-scale deforestation on precipitation in the monsoon regions: Remote versus local effects. *Proceedings of the National Academy of Sciences of the United States of America*, 112(11), 3257–3262. <https://doi.org/10.1073/pnas.1423439112>

- Devaraju, N., De Noblet-Ducoudré, N., Quesada, B., & Bala, G. (2018). Quantifying the relative importance of direct and indirect biophysical effects of deforestation on surface temperature and teleconnections. *Journal of Climate*, *31*(10), 3811–3829. <https://doi.org/10.1175/JCLI-D-17-0563.1>
- Di Vittorio, A. V., Mao, J., Shi, X., Chini, L., Hurtt, G., & Collins, W. D. (2018). Quantifying the effects of historical land cover conversion uncertainty on global carbon and climate estimates. *Geophysical Research Letters*, *45*(2), 974–982. <https://doi.org/10.1002/2017GL075124>
- Duveiller, G., Filippini, F., Ceglar, A., Bojanowski, J., Alkama, R., & Cescatti, A. (2021). Revealing the widespread potential of forests to increase low level cloud cover. *Nature Communications*, *12*(1), 4337. <https://doi.org/10.1038/s41467-021-24551-5>
- Duveiller, G., Hooker, J., & Cescatti, A. (2018). The mark of vegetation change on Earth's surface energy balance. *Nature Communications*, *9*(1), 679. <https://doi.org/10.1038/s41467-017-02810-8>
- Eyring, V., Bony, S., Meehl, G. A., Senior, C. A., Stevens, B., Stouffer, R. J., & Taylor, K. E. (2016). Overview of coupled model intercomparison Project phase 6 (CMIP6) experimental design and organization. *Geoscientific Model Development*, *9*(5), 1937–1958. <https://doi.org/10.5194/gmd-9-1937-2016>
- Foley, J. A., DeFries, R., Asner, G. P., Barford, C., Bonan, G., Carpenter, S. R., et al. (2005). Global consequences of land use. *Science*, *309*(5734), 570–574. <https://doi.org/10.1126/science.1111772>
- Forzieri, G., Alkama, R., Miralles, D. G., & Cescatti, A. (2017). Satellites reveal contrasting responses of regional climate to the widespread greening of Earth. *Science*, *356*(6343), 1180–1184. <https://doi.org/10.1126/science.aal1727>
- Ge, J., Guo, W., Pitman, A. J., De Kauwe, M. G., Chen, X., & Fu, C. (2019). The nonradiative effect dominates local surface temperature change caused by afforestation in China. *Journal of Climate*, *32*(14), 4445–4471. <https://doi.org/10.1175/JCLI-D-18-0772.1>
- Griscom, B. W., Adams, J., Ellis, P. W., Houghton, R. A., Lomax, G., Miteva, D. A., et al. (2017). Natural climate solutions. *Proceedings of the National Academy of Sciences of the United States of America*, *114*(44), 11645–11650. <https://doi.org/10.1073/pnas.1710465114>
- Hirsch, A. L., Pitman, A. J., & Kala, J. (2014). The role of land cover change in modulating the soil moisture-temperature land-atmosphere coupling strength over Australia. *Geophysical Research Letters*, *41*(16), 5883–5890. <https://doi.org/10.1002/2014GL061179>
- Houghton, R. A., & Hackler, J. L. (2003). Sources and sinks of carbon from land-use change in China. *Global Biogeochemical Cycles*, *17*(2), 1034. <https://doi.org/10.1029/2002GB001970>
- Hua, W., & Chen, H. (2013). Impacts of regional-scale land use/land cover change on diurnal temperature range. *Advances in Climate Change Research*, *4*(3), 166–172. <https://doi.org/10.3724/SP.J.1248.2013.166>
- Hua, W., Chen, H., Sun, S., & Zhou, L. (2015). Assessing climatic impacts of future land use and land cover change projected with the CanESM2 model. *International Journal of Climatology*, *35*(12), 3661–3675. <https://doi.org/10.1002/joc.4240>
- Huang, B., Hu, X., Fuglstad, G.-A., Zhou, X., Zhao, W., & Cherubini, F. (2020). Predominant regional biophysical cooling from recent land cover changes in Europe. *Nature Communications*, *11*(1), 1066. <https://doi.org/10.1038/s41467-020-14890-0>
- Huang, Y., Salama, M. S., Su, Z., Van der Velde, R., Zheng, D., Krol, M. S., et al. (2016). Effects of roughness length parameterizations on regional-scale land surface modeling of alpine grasslands in the Yangtze River Basin. *Journal of Hydrometeorology*, *17*(4), 1069–1085. <https://doi.org/10.1175/JHM-D-15-0049.1>
- Hurtt, G. C., Chini, L., Sahajpal, R., Frolking, S., Bodirsky, B. L., Calvin, K., et al. (2020). Harmonization of global land use change and management for the period 850–2100 (LUH2) for CMIP6. *Geoscientific Model Development*, *13*(11), 5425–5464. <https://doi.org/10.5194/gmd-13-5425-2020>
- Jackson, R. B., Randerson, J. T., Canadell, J. G., Anderson, R. G., Avissar, R., Baldocchi, D. D., et al. (2008). Protecting climate with forests. *Environmental Research Letters*, *3*(4), 044006. <https://doi.org/10.1088/1748-9326/3/4/044006>
- Jiang, Y., Wang, G., Liu, W., Erfanian, A., Peng, Q., & Fu, R. (2021). Modeled response of South American climate to three decades of deforestation. *Journal of Climate*, *34*(6), 2189–2203. <https://doi.org/10.1175/JCLI-D-20-0380.1>
- Juang, J. Y., Katul, G., Siqueira, M., Stoy, P., & Novick, K. (2007). Separating the effects of albedo from eco-physiological changes on surface temperature along a successional chronosequence in the southeastern United States. *Geophysical Research Letters*, *34*(21), L21408. <https://doi.org/10.1029/2007GL031296>
- Khanna, J., Medvigy, D., Fueglistaler, S., & Walko, R. (2017). Regional dry-season climate changes due to three decades of Amazonian deforestation. *Nature Climate Change*, *7*(3), 200–204. <https://doi.org/10.1038/nclimate3226>
- Kumar, S., Dirmeyer, P. A., Merwade, V., DelSole, T., Adams, J. M., & Niyogi, D. (2013). Land use/cover change impacts in CMIP5 climate simulations: A new methodology and 21st century challenges. *Journal of Geophysical Research: Atmospheres*, *118*(12), 6337–6353. <https://doi.org/10.1002/jgrd.50463>
- Laguë, M. M., & Swann, A. L. S. (2016). Progressive midlatitude afforestation: Impacts on clouds, global energy transport, and precipitation. *Journal of Climate*, *29*(15), 5561–5573. <https://doi.org/10.1175/JCLI-D-15-0748.1>
- Lawrence, D., & Vandecar, K. (2015). Effects of tropical deforestation on climate and agriculture. *Nature Climate Change*, *5*(1), 27–36. <https://doi.org/10.1038/nclimate2430>
- Lawrence, D. M., Hurtt, G. C., Arneth, A., Brovlin, V., Calvin, K. V., Jones, A. D., et al. (2016). The land use model intercomparison Project (LUMIP) contribution to CMIP6: Rational and experimental design [Dataset]. *Geoscientific Model Development*, *9*, 2973–2998. <https://doi.org/10.5194/gmd-9-2973-2016>
- Lee, X., Goulden, M. L., Hollinger, D. Y., Barr, A., Black, A., Bohrer, G., et al. (2011). Observed increase in local cooling effect of deforestation at higher latitudes. *Nature*, *479*(7373), 384–387. <https://doi.org/10.1038/nature10588>
- Lejeune, Q., Davin, E. L., Gudmundsson, L., Winckler, J., & Seneviratne, S. I. (2018). Historical deforestation locally increased the intensity of hot days in northern mid-latitudes. *Nature Climate Change*, *8*(5), 386–390. <https://doi.org/10.1038/s41558-018-0131-z>
- Lejeune, Q., Seneviratne, S. I., & Davin, E. L. (2017). Historical land-cover change impacts on climate: Comparative assessment of LUCID and CMIP5 multimodel experiments. *Journal of Climate*, *30*(4), 1439–1459. <https://doi.org/10.1175/JCLI-D-16-0213.1>
- Li, X., Chen, H., Hua, W., Ma, H., Li, X., Sun, S., et al. (2022). Modeling the effects of realistic land cover changes on land surface temperatures over China. *Climate Dynamics*. <https://doi.org/10.1007/s00382-022-06635-0>
- Li, X., Chen, H., Wei, J., Hua, W., Sun, S., Ma, H., et al. (2018). Inconsistent responses of hot extremes to historical land use and cover change among the selected CMIP5 models. *Journal of Geophysical Research: Atmospheres*, *123*(7), 3497–3512. <https://doi.org/10.1002/2017JD028161>
- Li, Y., De Noblet-Ducoudré, N., Davin, E. L., Motesharrei, S., Zeng, N., Li, S., & Kalnay, E. (2016). The role of spatial scale and background climate in the latitudinal temperature response to deforestation. *Earth System Dynamics*, *7*(1), 167–181. <https://doi.org/10.5194/esd-7-167-2016>
- Li, Y., Wang, T., Zeng, Z., Peng, S., Lian, X., & Piao, S. (2016). Evaluating biases in simulated land surface albedo from CMIP5 global climate models. *Journal of Geophysical Research: Atmospheres*, *121*(11), 6178–6190. <https://doi.org/10.1002/2016JD024774>
- Li, Y., Zhao, M., Mildrexler, D. J., Motesharrei, S., Mu, Q., Kalnay, E., et al. (2016). Potential and Actual impacts of deforestation and afforestation on land surface temperature. *Journal of Geophysical Research: Atmospheres*, *121*(24), 14372–14414. <https://doi.org/10.1002/2016JD024969>

- Li, Y., Zhao, M. S., Motesharrei, S., Mu, Q. Z., Kalnay, E., & Li, S. C. (2015). Local cooling and warming effects of forests based on satellite observations. *Nature Communications*, 6(1), 6603. <https://doi.org/10.1038/ncomms7603>
- Lian, X., Jeong, S., Park, C.-E., Xu, H., Li, L. Z. X., Wang, T., et al. (2022). Biophysical impacts of northern vegetation changes on seasonal warming patterns. *Nature Communications*, 13(1), 3925. <https://doi.org/10.1038/s41467-022-31671-z>
- Liao, W., Rigden, A. J., & Li, D. (2018). Attribution of local temperature response to deforestation. *Journal of Geophysical Research: Biogeosciences*, 123(5), 1572–1587. <https://doi.org/10.1029/2018JG004401>
- Liu, J., Hagan, D. F. T., & Liu, Y. (2021). Global land surface temperature change (2003–2017) and its relationship with climate drivers: AIRS, MODIS, and ERA5-land based analysis. *Remote Sensing*, 13(1), 44. <https://doi.org/10.3390/rs13010044>
- Liu, Y. Y., Van Dijk, A. I. J. M., De Jeu, R. A. M., Canadell, J. G., McCabe, M. F., Evans, J. P., & Wang, G. (2015). Recent reversal in loss of global terrestrial biomass. *Nature Climate Change*, 5, 470–474. <https://doi.org/10.1038/nclimate2581>
- Liu, Y. Y., Van Dijk, A. I. J. M., McCabe, M. F., Evans, J. P., & De Jeu, R. A. M. (2013). Global vegetation biomass change (1988–2008) and attribution to environmental and human drivers. *Global Ecology and Biogeography*, 22(6), 692–705. <https://doi.org/10.1111/geb.12024>
- Lorantny, M. M., Berner, L. T., Goetz, S. J., Jin, Y., & Randerson, J. T. (2014). V vegetation controls on northern high latitude snow-albedo feedback: Observations and CMIP5 model simulations. *Global Change Biology*, 20(2), 594–606. <https://doi.org/10.1111/geb.12391>
- Luo, X., Ge, J., Guo, W., Fan, L., Chen, C., Liu, Y., & Yang, L. (2022). The biophysical impacts of deforestation on precipitation: Results from the CMIP6 model intercomparison. *Journal of Climate*, 35(11), 3293–3311. <https://doi.org/10.1175/JCLI-D-21-0689.1>
- Luyssaert, S., Jammot, M., Stoy, P. C., Estel, S., Pongratz, J., Ceschia, E., et al. (2014). Land management and land-cover change have impacts of similar magnitude on surface temperature. *Nature Climate Change*, 4(5), 389–393. <https://doi.org/10.1038/nclimate2196>
- Mahmood, R., Pielke Sr, R. A., Hubbard, K. G., Dirmeyer, P. A., McAlpine, C., Carleton, A. M., et al. (2014). Land cover changes and their biogeophysical effects on climate. *International Journal of Climatology*, 34(4), 929–953. <https://doi.org/10.1002/joc.3736>
- Malyshev, S., Shevliakova, E., Stouffer, R. J., & Pacala, S. W. (2015). Contrasting local versus regional effects of land-use-change-induced heterogeneity on historical climate: Analysis with the GFDL Earth system model. *Journal of Climate*, 28(13), 5448–5469. <https://doi.org/10.1175/JCLI-D-14-00586.1>
- Mauritsen, T., Bader, J., Becker, T., Behrens, J., Bittner, M., Brokopf, R., et al. (2019). Developments in the MPI-M Earth system model version 1.2 (MPI-ESM 1.2) and its response to increasing CO₂. *Journal of Advances in Modeling Earth Systems*, 11(4), 998–1038. <https://doi.org/10.1029/2018MS001400>
- Meier, R., Davin, E. L., Bonan, G. B., Lawrence, D. M., Hu, X., Duveiller, G., et al. (2022). Impacts of a revised surface roughness parameterization in the community land model 5.1. *Geoscientific Model Development*, 15(6), 2365–2393. <https://doi.org/10.5194/gmd-15-2365-2022>
- Perugini, L., Caporaso, L., Marconi, S., Cescatti, A., Quesada, B., De Noblet-Ducoudré, N., et al. (2017). Biophysical effects on temperature and precipitation due to land cover change. *Environmental Research Letters*, 12(5), 053002. <https://doi.org/10.1088/1748-9326/aa6b3f>
- Pielke, S. R. A., Pitman, A., Niyogi, D., Mahmood, R., McAlpine, C., Hossain, F., et al. (2011). Land use/land cover changes and climate: Modeling analysis and observational evidence. *Wiley Interdisciplinary Reviews: Climate Change*, 2(6), 828–850. <https://doi.org/10.1002/wcc.144>
- Pitman, A. J., De Noblet-Ducoudré, N., Avila, F. B., Alexander, L. V., Boisier, J.-P., Brovkin, V., et al. (2012). Effects of land cover change on temperature and rainfall extremes in multi-model ensemble simulations. *Earth System Dynamics*, 3(2), 213–231. <https://doi.org/10.5194/esd-3-213-2012>
- Pitman, A. J., De Noblet-Ducoudré, N., Cruz, F. T., Davin, E. L., Bonan, G. B., Brovkin, V., et al. (2009). Uncertainties in climate responses to past land cover change: First results from the LUCID intercomparison study. *Geophysical Research Letters*, 36(14), L14814. <https://doi.org/10.1029/2009GL039076>
- Pongratz, J., Reick, C., Raddatz, T., & Claussen, M. (2008). A reconstruction of global agricultural areas and land cover for the last millennium. *Global Biogeochemical Cycles*, 22(3), GB3018–n. <https://doi.org/10.1029/2007GB003153>
- Pongratz, J., Reick, C. H., Raddatz, T., & Claussen, M. (2010). Biogeophysical versus biogeochemical climate response to historical anthropogenic land cover change. *Geophysical Research Letters*, 37(8), L08702. <https://doi.org/10.1029/2010GL043010>
- Pongratz, J., Schwingshackl, C., Bultan, S., Obermeier, W., Havermann, F., & Guo, S. (2021). Land use effects on climate: Current state, recent progress, and emerging topics. *Current Climate Change Reports*, 7(4), 99–120. <https://doi.org/10.1007/s40641-021-00178-y>
- Portmann, R., Beyerle, U., Davin, E., Fischer, E. M., De Hertog, S., & Schemm, S. (2022). Global forestation and deforestation affect remote climate via adjusted atmosphere and ocean circulation. *Nature Communications*, 13(1), 5569. <https://doi.org/10.1038/s41467-022-33279-9>
- Rigden, A. J., & Li, D. (2017). Attribution of surface temperature anomalies induced by land use and land cover changes. *Geophysical Research Letters*, 44(13), 6814–6822. <https://doi.org/10.1002/2017GL073811>
- Rotenberg, E., & Yakir, D. (2010). Contribution of semi-arid forests to the climate system. *Science*, 327(5964), 451–454. <https://doi.org/10.1126/science.1179998>
- Runyan, C. W., D'Odorico, P., & Lawrence, D. (2012). Physical and biological feedbacks of deforestation. *Reviews of Geophysics*, 50(4), RG4006. <https://doi.org/10.1029/2012RG000394>
- Spracklen, D. V., Baker, J. C. A., Garcia-Carreras, L., & Marsham, J. (2018). The effects of tropical vegetation on rainfall. *Annual Review of Environment and Resources*, 43(1), 193–218. <https://doi.org/10.1146/annurev-environ-102017-030136>
- Tafasca, S., Ducharme, A., & Valentin, C. (2020). Weak sensitivity of the terrestrial water budget to global soil texture maps in the ORCHIDEE land surface model. *Hydrology and Earth System Sciences*, 24(7), 3753–3774. <https://doi.org/10.5194/hess-24-3753-2020>
- Thackeray, C. W., Derksen, C., Fletcher, C. G., & Hall, A. (2019). Snow and climate: Feedbacks, drivers, and indices of change. *Current Climate Change Reports*, 5(4), 322–333. <https://doi.org/10.1007/s40641-019-00143-w>
- Tölle, M. H., Engler, S., & Panitz, H.-J. (2017). Impact of abrupt land cover changes by tropical deforestation on Southeast Asian climate and agriculture. *Journal of Climate*, 30(7), 2587–2600. <https://doi.org/10.1175/JCLI-D-16-0131.1>
- Van der Werf, G., Morton, D. C., DeFries, R. S., Olivier, J. G. J., Kasibhatla, P. S., Jackson, R. B., et al. (2009). CO₂ emissions from forest loss. *Nature Geoscience*, 2(11), 737–738. <https://doi.org/10.1038/ngeo671>
- Van Marle, M. J. E., Van der Werf, G. R., De Jeu, R. A. M., & Liu, Y. Y. (2016). Annual South American forest loss estimates based on passive microwave remote sensing (1990–2010). *Biogeosciences*, 13(2), 609–624. <https://doi.org/10.5194/bg-13-609-2016>
- Wang, G., Sun, S., & Mei, R. (2011). Vegetation dynamics contributes to the multi-decadal variability of precipitation in the Amazon region. *Geophysical Research Letters*, 38(19), L19703. <https://doi.org/10.1029/2011GL049017>
- Werth, D., & Avissar, R. (2002). The local and global effects of Amazon deforestation. *Journal of Geophysical Research*, 107(D20), 8087. <https://doi.org/10.1029/2001JD000717>
- Winckler, J., Lejeune, Q., Reick, C. H., & Pongratz, J. (2019). Nonlocal effects dominate the global mean surface temperature response to the biogeophysical effects of deforestation. *Geophysical Research Letters*, 46(2), 745–755. <https://doi.org/10.1029/2018GL080211>
- Winckler, J., Reick, C. H., Bright, R. M., & Pongratz, J. (2019). Importance of surface roughness for the local biogeophysical effects of deforestation. *Journal of Geophysical Research: Atmospheres*, 124(15), 8605–8618. <https://doi.org/10.1029/2018JD030127>

- Winckler, J., Reick, C. H., Luyssaert, S., Cescatti, A., Stoy, P. C., Lejeune, Q., et al. (2019). Different response of surface temperature and air temperature to deforestation in climate models. *Earth System Dynamics*, *10*(3), 473–484. <https://doi.org/10.5194/esd-10-473-2019>
- Winckler, J., Reick, C. H., & Pongratz, J. (2017). Robust identification of local biogeophysical effects of land-cover change in a global climate model. *Journal of Climate*, *30*(3), 1159–1176. <https://doi.org/10.1175/JCLI-D-16-0067.1>
- Xu, R., Li, Y., Teuling, A. J., Zhao, L., Spracklen, D. V., Garcia-Carreras, L., et al. (2022). Contrasting impacts of forests on cloud cover based on satellite observations. *Nature Communications*, *13*(1), 670. <https://doi.org/10.1038/s41467-022-28161-7>
- Yu, M., Wang, G., & Pal, J. S. (2016). Effects of vegetation feedback on future climate change over West Africa. *Climate Dynamics*, *46*(11–12), 3669–3688. <https://doi.org/10.1007/s00382-015-2795-7>
- Yuan, K., Zhu, Q., Zheng, S., Zhao, L., Chen, M., Riley, W. J., et al. (2021). Deforestation reshapes land-surface energy-flux partitioning. *Environmental Research Letters*, *16*(2), 024014. <https://doi.org/10.1088/1748-9326/abd8f9>
- Zeng, Z., Piao, S., Li, L. Z. X., Zhou, L., Ciais, P., Wang, T., et al. (2017). Climate mitigation from vegetation biophysical feedbacks during the past three decades. *Nature Climate Change*, *7*(6), 432–436. <https://doi.org/10.1038/nclimate3299>
- Zhang, M., Lee, X., Yu, G., Han, S., Wang, H., Yan, J., et al. (2014). Response of surface air temperature to small-scale land clearing across latitudes. *Environmental Research Letters*, *9*(3), 034002. <https://doi.org/10.1088/1748-9326/9/3/034002>
- Zhang, W., Xu, Z., & Guo, W. (2016). The impacts of land-use and land-cover change on tropospheric temperatures at global and regional scales. *Earth Interactions*, *20*(7), 1–23. <https://doi.org/10.1175/EI-D-15-0029.1>
- Zhao, K., & Jackson, R. B. (2014). Biophysical forcings of land-use changes from potential forestry activities in North America. *Ecological Monographs*, *84*(2), 329–353. <https://doi.org/10.1890/12-1705.1>
- Zhou, L. (2021). Diurnal asymmetry of desert amplification and its possible connections to planetary boundary layer height: A case study for the Arabian Peninsula. *Climate Dynamics*, *56*(9–10), 3131–3156. <https://doi.org/10.1007/s00382-021-05634-x>
- Zhou, L., Dickinson, R. E., Tian, Y., Vose, R. S., & Dai, Y. (2007). Impact of vegetation removal and soil aridation on diurnal temperature range in a semiarid region: Application to the Sahel. *Proceedings of the National Academy of Sciences of the United States of America*, *104*(46), 17937–17942. <https://doi.org/10.1073/pnas.0700290104>
- Zhou, L., Dickinson, R. E., Tian, Y., Zeng, X., Dai, Y., Yang, Z.-L., et al. (2003). Comparison of seasonal and spatial variations of albedos from moderate-resolution imaging spectroradiometer (MODIS) and common land model. *Journal of Geophysical Research*, *108*(D15), 4488. <https://doi.org/10.1029/2002JD003326>
- Zwiers, F. W., & Von Storch, H. (1995). Taking serial correlation into account in tests of the mean. *Journal of Climate*, *8*(2), 336–351. [https://doi.org/10.1175/1520-0442\(1995\)008<0336:tsciai>2.0.co;2](https://doi.org/10.1175/1520-0442(1995)008<0336:tsciai>2.0.co;2)